İZMİR KATİP ÇELEBİ UNIVERSITY ★ GRADUATE SCHOOL OF NATURAL AND APPLIED SCIENCES

BORON DOPED TITANIUM DIOXIDE NANOTUBE ARRAYS: PRODUCTION, CHARACTERIZATION AND PHOTOCATALYTIC PROPERTIES

M.Sc. THESIS

KÜBRA BİLGİN

Department of Materials Science and Engineering

Thesis Advisor: Asst. Prof. Dr. Mustafa EROL

June 2016

İZMİR KATİP ÇELEBİ UNIVERSITY ★ GRADUATE SCHOOL OF NATURAL AND APPLIED SCIENCES

BORON DOPED TITANIUM DIOXIDE NANOTUBE ARRAYS: PRODUCTION, CHARACTERIZATION AND PHOTOCATALYTIC PROPERTIES

M.Sc. THESIS

KÜBRA BİLGİN

Department of Materials Science and Engineering

Thesis Advisor: Asst. Prof. Dr. Mustafa EROL

June 2016

İZMİR KATİP ÇELEBİ ÜNİVERSİTESİ ★ FEN BİLİMLERİ ENSTİTÜSÜ

BOR KATKILI TİTANYUM DİOKSİT NANOTÜP YAPILAR: ÜRETİM KARAKTERİZASYON VE FOTOKATALİTİK ÖZELLİKLER

YÜKSEK LİSANS TEZİ

KÜBRA BİLGİN

Malzeme Bilimi ve Mühendisliği Bölümü

Tez Danışmanı: Yrd. Doç. Dr. Mustafa EROL

Haziran 2016

Kübra BİLGİN, a M.Sc. student of İzmir Katip Çelebi University student ID Y120111017, successfully defended the thesis entitled "Boron doped titanium oxide nanotube arrays: production, characterization and photocatalytic properties", which she prepared after fulfilling the requirements specified in the associated legislations, before the jury whose signatures are below.

Thesis Advisor: Asst. Prof. Dr. Mustafa EROL
Izmir Kâtip Çelebi University

Jury Members: Assoc. Prof. Dr. Mücahit Sütçü
Izmir Katip Çelebi University

Assoc. Prof. Dr. Ömer MERMER
Ege University

Date of Submission : 03.06.2016

Date of Defense : 03.06.2016

FOREWORD

Primarily I would thank God for being able to complete my thesis with success and secondly I owe many people a debt of gratitude. I would like to express my advisor Asst. Prof. Dr. Mustafa Erol sincere thanks for his initiative in preparing the working environment and his guidance with moral and material support and good advices. I would like to express my gratitude to Res. Assist. Tuncay DİKİCİ for good advices and letting me use his equipment in laboratory.

I would like to thank my workfellow MSc. Student Emine BAŞALAN for her help on orientation to EMUM. I present my thanks to doctoral student Çağlar ÖZER for teaching how to use diffuse reflectance spectroscopy device. I present my thanks expert Metin YURDDAŞKAL for giving advices about UV-Vis Spectrophotometer device. I present my thanks to Res. Assist. Kadir Cihan Tekin for good advices and help on grinding-polishing process and letting me use his equipment and Res. Assist. Haydar Kahraman for XRD analysis. I present my thanks to Res. Assist. Selim DEMİRCİ for AFM analysis.

I would like to thank my father and sister for understanding and their continuous moral support during my thesis and I am grateful to them for believing I could carry through my thesis.

This study was founded by Izmir Katip Celebi University Scientific Research Projects Coordinatorship with project code: 2015-ÖNP-MÜMF-0011.

03.06.2016 Kübra BİLGİN

TABLE OF CONTENTS

Page

ABREVIATIONS

TNTAs	: Titanium dioxide nanotube arrays
B-TNTAs	: Boron doped titanium dioxide nanotube arrays
SC	: Semiconductor
CB	: Conduction band
VB	: Valance band
OCs	: Organic contaminants
AOPs	: Advanced oxidation process
UV	: Ultra viole
EH	: Electrolyte prepared with only hydrogen floride in water
EHOx	: Electrolyte prepared with both hydrogen floride and oxalic acid in water
EHB	: Electrolyte prepared with both hydrogen floride and sodium tetra fluoro borate in water.
EHOxB	: Electrolyte prepared with all hydrogen floride, oxalic acid and sodium tetra fluoro borate in water.
XRD	: X-Ray Diffraction
SEM	: Scanning electron microscopy
EDS	: Energy-dispersive X-Ray spectroscopy
AFM	: Atomic force microscopy
SPM	: Scanning probe microscopes
DRS	: Diffuse reflectance spectroscopy
MB	: Methylene blue solution

LIST OF TABLES

LIST OF FIGURES

LIST OF SYMBOLS

E_g	: Band gap energy
ħ	: Planks constant
c	: Speed of light
λ	: Wavelength
A	: Absorbance
I_0	: Intensity of the light passing through refence cell
I	: Intensity of the light passing through sample cell
ε	: Molar absorptivity
L	: Length of solution the light passes through (cm)
C	: Concentration of solution (mol/L)
R^2	: Standard deviation value
k	: Kinetic constant (min^{-1})

BORON DOPED TITANIUM DIOXIDE NANOTUBE ARRAYS: PRODUCTION, CHARACTERIZATION AND PHOTOCATALYTIC PROPERTIES

SUMMARY

Photocatalytic degradation and complete mineralization of toxic organic compounds in water, soil, and air in the presence of semiconductor materials have received much attention over the last decades. Electronic structure of semiconductors is characterized by a filled valence band and an empty conduction band. When the semiconductor is irradiated with light of sufficient energy corresponding to or exceeding its band gap, an electron is promoted into the conduction band, leaving a hole in the valence band. The electrons and holes are good reductants and powerful oxidants, respectively, and they can initiate redox reactions on the semiconductor surface. Titanium dioxide (TiO_2) as a semiconductor is considered the most promising photocatalyst due to its high efficiency, chemical stability and non-toxicity. Due to the fact that in this study, titanium dioxide nanotube arrays fabricated by potentiostatic anodization of titanium that offers a large internal surface area. TiO_2 nanotube arrays have been found to possess outstanding charge transport and carrier lifetime properties enabling a variety of advanced applications, including their usage as sensors, dye sensitized solar cells, hydrogen generators, photocatalysts, and super capacitors. However, the use of TiO_2 is restricted by its wide band gap (3.2-3.6 eV), which requires ultraviolet irradiation for photocatalytic activation (λ <387 nm). In addition, UV light include accounts for only about 5 % of solar energy; visible light, 45 %. The shift of the optical response of TiO_2 from UV to the visible spectral range will have a profound positive effect on the efficient use of solar energy in photocatalytic reactions. Thus, much effort has been directed toward the development of visible light-active photocatalysts. With this manner aim of this study is to reduce the band gap energy of TiO_2 nanotubes through boron (B) doping. Both pure and doped TiO_2 nanotube arrays (TNTAs) were fabricated on pure titanium substrates and stable nanotube production was performed by anodization process. Electrochemical anodization process was followed by a heat treatment which led the transformation of amorphous structure in to crystalline anatase phase. Samples were characterized by X-ray diffraction (XRD), diffuse reflectance absorption spectroscopy (DRS), atomic force microscopy (AFM) and scanning electron microscopy/energy-dispersive X-ray spectroscopy (SEM/EDS). Finally, photocatalytic efficiencies were tested under UV light and photocatalytical degradation and kinetics were evaluated by UV-Visible spectrophotometer.

BOR KATKILI TİTANYUM DİOKSİT NANOTÜP YAPILAR: ÜRETİM KARAKTERİZASYON VE FOTOKATALİTİK ÖZELLİKLER

ÖZET

Yaşam kaynağı olan su, toprak ve havanın içeriğine karışan zehirli organic bileşiklerin yarıiletken malzemeler varlığında fotokatalitik parçalanması ve mineralizasyonu son yıllarda çok ilgi görmüştür ve görmeye devam etmektedir. Yarı iletkenlerin elektronik yapısı elektron bant yapısı ile yani elektronca dolu valans bant ve boş iletim bant ile tanımlanır. Bir yarı iletken yeterli ışığa maruz bırakıldığında valans bantta bulunan elektron enerji kazanır ve valans bandında boşluk oluşarak elektron iletim bandına uyarılır. Bu elektron ve boşluklar yarı iletken yüzeyinde redoks reaksiyonlarını başlatabilir derecede iyi indirgeyici ve güçlü oksitleyici görevi görürler. Yüksek verim, kimyasal kararlılık ve toksik olmayan özelliklere sahip titanyum dioksit bir yarı iletken olarak en umut vaat edici fotokatalizördür. Bu nedenle bu çalışmada, geniş yüzey alanı oluşturma imkanı sağlayan anotlama yöntemi ile titanyum dioksit nanotüp yüzeyler üretilmiştir. Titanyum dioksit (TiO_2) geniş bir bant aralığına sahiptir (3.2-3.6 eV) ve bu bant aralığı titanyum dioksidin ultra-viole (UV) ışık altında fotokatalitik etkinlik göstermesine olanak sağlamaktadır. Güneş enerjisi sadece % 5 oranında UV ışık ve % 45 oranında görünür ışık içermektedir. Buna bağlı olarak, titanyum dioksidin UV bölgedeki etkinliğinin görünür spektral aralığa kaydırılmasının fotokatalitik reaksiyonlarda güneş enerjisinin verimli kullanımı konusunda olumlu etkisi olacaktır. Görünür ışıkta aktif fotokatalizör geliştirilmesine yönelik bir çok çalışma mevcuttur. Bu çalışmanın amacı titanyum dioksidin bant aralığını düşürmek için bor (B) katkılandırması yapmaktır. Katkısız ve bor katkılı titanyum dioksit nanotüp yüzeyler saf titanyum üzerinde üretilmiştir ve kararlı nanotüp üretimi anotlama prosesiyle gerçekleştirilmiştir. Elektrokimyasal anotlama işlemi sonrası oluşan amorf yapıdan kararlı anataz kristal fazına dönüşümü sağlamak için ısıl işlem uygulanmıştır. Numunelerin karakterizasyonu X-ışını kırınımı (XRD),dağılan yansıma absorbsiyon spektroskopi (DRS), atomic kuvvet mikroskobu (AFM) ve taramalı elektron mikroskobu/enerji dağılımlı X-ışını spektroskopisi (SEM/EDS) analiz cihazları ile yapılmıştır. Son olarak fotokatalitik etkinlik UV ışık altında test edilip, fotokatalitik parçalanma UV-görünür bölge sprectrofotometre cihazıyla saptanmıştır.

1. INTRODUCTION

The world's most crucial natural resource, water, is under threat of various contaminants, causing water crisis. The disposal of toxic contaminants, such as dyes and phenolic compounds which are harmful for environment, hazardous to humans, and difficult to degrade, are pervasively associated with industrial development and these contaminants are frequently found in the industrial effluents [1]. Chemical precipitation, filtration, electro-deposition, ion-exchange adsorption, and membrane systems are some of the conventional methods for water treatment. However, sometimes these methods may not be very effective, because they are either slow or non-destructive enough to some or most persistent organic pollutants. In addition to previously mentioned techniques, advanced oxidation processes (AOPs) has been utilized so as to treat waste water for a while. AOPs are the common name of several chemical oxidation methods used to remediate substances that are highly resistant to biological degradation. On the other hand; semiconductor photocatalysis (light assisted oxidation process) is a popular technique that has the great potential to control the organic contaminants in water. Semiconductor photocatalysis has attracted a great deal of attention as a useful technique of water splitting and decontamination treatment in polluted water [2]. Photocatalysts speed up chemical oxidation reactions by utilization of photons and photocatalysis is an excellent way to perform many reduction and oxidation reactions at room temperature. It is found to be an economical and sustainable method for the removal of various pollutants from gas and liquid streams by oxidation of such aromatics, as colorants, carbon monoxide (CO) etc. The development of photocatalysis has been the worthy of attention in recent decades due to its application in a broad range of research areas, including especially environmental and energy-related fields [3–5]. Photolysis of water was firstly reported by Fujishima and Honda in 1972 [6]. The photocatalytic properties of some materials have been used to convert solar energy into chemical energy to oxidize or reduce materials to obtain useful materials including hydrogen [7] and hydrocarbons [8], and to remove pollutants and bacteria [9-14] on wall

surfaces, in air and water [1]. Among the photocatalysts, TiO_2 has been the one which is widely studied and used in applications because of its remarkable oxidizing abilities [15-18] for the decomposition of organic pollutants [15,16], superhydrophilicity, chemical stability, long durability, non-toxicity, low cost, and transparency to visible light. The photocatalytic activity of various forms of TiO_2, such as powders [8, 10-12], film [7, 14], nanotubes [18-44] and doped TiO_2 [20, 32, 38-44, 46-57] have been evaluated. Among the cited forms, nanotube structures have higher specific surface areas which are important for photocatalysis. TiO_2 nanotube arrays (TNTAs) have been produced by a number of methods. These include: using a nanoporous alumina as a template [19-22], sol-gel transcription processes using organo-gelator templates [23, 24], seeded growth mechanisms [25], hydrothermal techniques [26–28], and anodization process [29–36]. If compared; anodization can be located one step ahead due to such advantages as; superior control over the nanotube dimensions, cost effectiveness and ease in production [29–36].

TiO_2 is activated under UV light irradiation (λ<387 nm) because of its larger band gap of 3,15-3.6 eV [37]. As known, UV light accounts for only a small fraction (5%) of the solar spectrum. With this manner extending TiO_2s' spectral response into the visible region and improving its photocatalytic efficiency has been an important issue [38]. Incorporating some elements or structures in to TiO_2 structure, such as N [39], C [40], P [41], Mo-Sb-S [42], CdSe [43], CdS [44,45], RuO [46], CdO [47], Cr [48], Mo-N [49], N-V [50], W-N [38], Ag [51], C-V [52], Cu [53], Ti^{+3}-C [54]and B [55, 57] and B-F [58] were found to be efficient way of band gap engineering to excite its photocatalytic activity under visible light. Recently, boron-doping begins to attract attention in electrochemical and functional materials applications because it is prompting the creation of electron acceptor level [55]. Actually, boron atoms can substitute oxygen atoms in the TiO_2 lattice and the p orbital of B is mixed with 2p orbital of O, which causes the band gap narrowing and as a result, shifts the optical response to the visible range. Therefore, it is also a promising path towards photocatalysis under visible light [55].The preparation of B-doped TiO_2 powders by sol–gel method has been reported [56, 57]. Another study has been reported on boron incorporation by chemical vapor deposition on anodized TNTAs [58]. Another researcher formed boron doped TNTAs (B-TNTAs) by electrochemical oxidation of titanium sheet in the electrolyte containing boron [59].

The main propose of this thesis is to produce catalysts by anodic oxidation which can be active under the solar light for purification of industrial waste water. Thus, B-TNTAs will be fabricated by anodic oxidation and they will be elaborately investigated by means of structure, morphology, optical, elemental and photocatalytical analysis. If the similar studies in literature considered it will be observed that they interested in different mediums to degrade instead of methylene blue and they are lack of detailed characterization. For example, Yaling Su et al carried out F–B-co-doping successfully by annealing the anodized TNTAs through chemical vapor deposition (CVD) in order to degrade methylene orange [58]. Na Lu et al, fabricated the boron-doped TNTAs by potentiostatic anodization of titanium in an aqueous electrolyte containing fluoride ion and sodium fluoroborate ($NaBF_4$) for the removal of atrazine [59], Yaling Su et al, applied CVD to doped boron into TiO_2 nanotubes anodized Ti in $C_2H_2O_4 \cdot 2H_2O$+NH_4F electrolyte so as to degrade methylene orange [55]. However, to the best of our knowledge, anodization parameters, kinetics and relationship between structure and photocatalytic activity on methylene blue has not been investigated in details yet.

In this study, TNTAs on the titanium substrates were be fabricated by electrochemical anodization at different anodization parameters (voltage, time and hydroflouric acid concentration of electrolyte). Subsequent to the anodic oxidation, the anodized substrates were annealed to improve the crystallinity and phase transformation. Optimum TNTAs production parameters were evaluated by prior characterization steps to enlighten further boron doping processes. After optimum parameters were determined, TNTAs doped with B were generated in an aqueous solution containing hydrofluoric acid (HF), oxalic acid ($H_2C_2O_4.2H_2O$) and sodium fluoro borate ($NaBF_4$) at room temperature. As-prepared B doped TNT structure was characterized by field emission scanning electron microscopy (SEM), energy dispersive x-ray analysis (EDS), x-ray diffraction (XRD), diffuse reflectance spectroscopy (DRS). The photocatalytic activity and kinetics of B doped TNTAs for the degradation of methylene blue (MB) under UV light irradiation was determined.

2. THEORITICAL BACKGROUND

2.1. Semiconductivity and Photocatalysis

A semiconductor is a material, usually a solid chemical element or compound that can conduct electricity under some conditions, making it a good medium for the control of electrical current [60]. Its conductance varies depending on the current or voltage applied to a control electrode, or on the intensity of irradiation by infrared (IR), visible light, ultraviolet (UV), or X rays.

The electrical conductivity of the semiconducting materials is not as high as that of the metals; nevertheless, they have some unique electrical characteristics that render them especially useful [60]. The electrical properties of these materials are extremely sensitive to the presence of even minute concentrations of impurities. Semiconductor is a solid with a full band and a small band gap. Intrinsic semiconductivity: Small conductivity created by the thermal/photo excitations electrons from valence to conduction band [60].

Almost every commercial semiconductor materials are extrinsic. Extrinsic semiconductivity: Small conductivity created by a doping through loss/gain of electrons from valence/conduction bands, respectively [60]. P-type semiconductor: Positive holes created in the insulator by an electron poor dopant. N-type semiconductor: Electron holes created in the insulator by an electron rich dopant.

The specific properties of a semiconductor depend on the impurities, or *dopants*, added to it. An *n-type* semiconductor carries current mainly in the form of negatively-charged electrons, in a manner similar to the conduction of current in a wire. A *p-type* semiconductor carries current predominantly as electron deficiencies called holes. A hole has a positive electric charge, equal and opposite to the charge

on an electron. In a semiconductor material, the flow of holes occurs in a direction opposite to the flow of electrons [60].

Elemental semiconductors include antimony, arsenic, boron, carbon, germanium, selenium, silicon, sulfur, and tellurium. Silicon is the best-known of these, forming the basis of most integrated circuits. Common semiconductor compounds include gallium arsenide (GaAs), indium antimonide (InSb), and *the oxides of most metals*. Of these, GaAs is widely used in low-noise, high-gain, weak signal amplifying devices. Wide band gap semiconductors such as SnO_2, TiO_2, and ZnO etc. have been paying a great deal of attention due to their potential applications for next-generation electronic and optoelectronic devices [61-63].

However, TiO_2 electrodes have been extensively investigated for their superior semiconducting material properties [3], and among the TiO_2 photoelectrodes with various morphologies and architectures, the anodic TiO_2 nanotube array exhibits more promising photochemical and photocatalytic properties, because of its nanotube-array architecture, which enhances the electron percolation pathway for vectorial charge transfer, promotes ion diffusion in the semiconductor /electrolyte interface [64-66], and restrains photogenerated electron–hole pairs from recombination [67].The highly ordered architecture of vertically aligned nanotubes creates a large surface-to-area ratio that is ideally suited for optical and catalytic performance. As a semiconductor material TiO_2 catalysts were considerably used for degradation of polluter organic compounds by photocatalysis in literature.

The word photocatalysis is a composite word which is composed of two parts, “photo” and “catalysis”. Catalysis is the process by which a substance speeds up a chemical reaction without being consumed or altered in the end of process [68]. This substance is known as the catalyst which increases the rate of a reaction by reducing the activation energy.

Generally speaking, photocatalysis is a reaction which uses light to activate a substance which modifies the rate of a chemical reaction without being involved itself. And the photocatalyst is the substance which can modify the rate of chemical reaction using light irradiation.

Chlorophyll of plants is a typical natural photocatalyst. The difference between chlorophyll photocatalyst to man-made nano TiO_2 photocatalyst is, usually chlorophyll captures sunlight to turn water and carbon dioxide into oxygen and glucose, but on the contrary photocatalyst TiO_2 gives rise to strong oxidation agent and electronic holes to breakdown the organic matter to carbon dioxide and water. This difference is illustrated in Figure2.1.

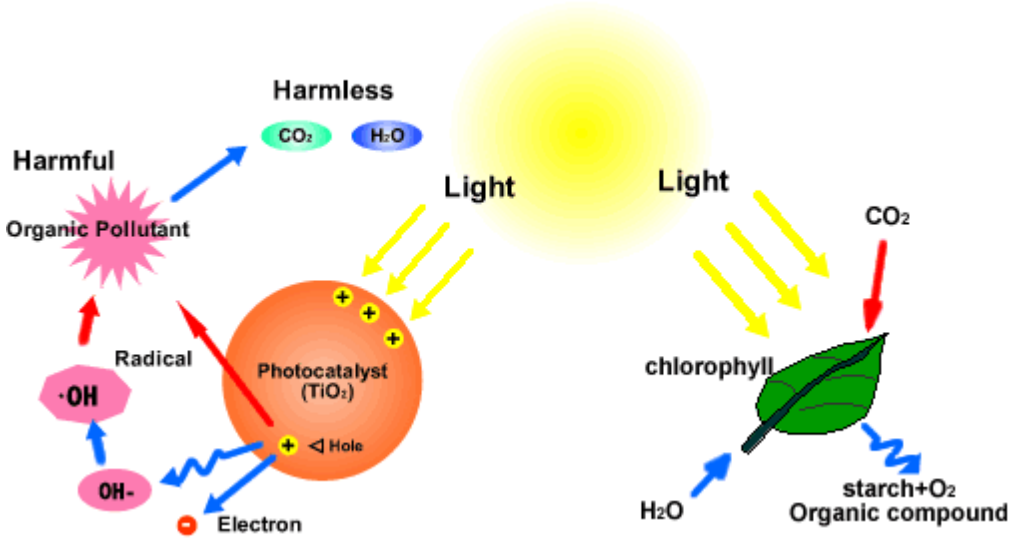

Figure 2.1: Schematic illustration of the formation of photocatalytic reaction belonging to both man-made nano TiO2 catalysts and natural chlorophyll catalysts [69].

2.1.1. Photocatalytical degradation mechanisms

The basic principle of photocatalytical degradation mechanisms is that UV light upgrades electrons from the valance band to the conduction band, and holes and electrons will be separated. The holes and electrons reach the semiconductor-environment interface, and react with appropriate redox species in the environment. In that time, reactive species are arisen from the surrounding water by charge exchange at the valance band and at the conduction band as represented in Figure 2.2. These radicals and peroxide ions are able to virtually oxidize all organic materials to CO_2 and H_2O. Furthermore, at the valence band, direct h^+ transfer to adsorbed species to initiate decomposition may also be considered [70]. The reactions that are promoted with the absorption of photon (hυ) and photocatalytical degradation mechanism are given below.

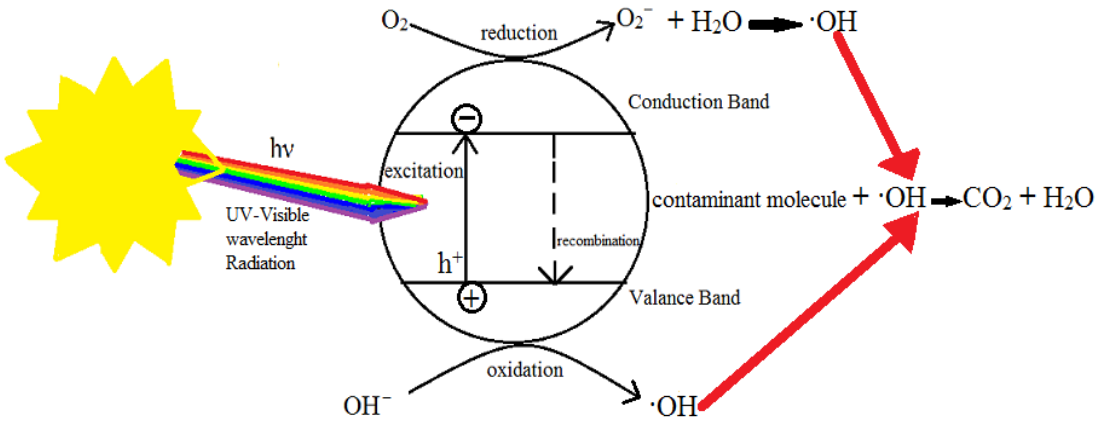

Figure 2.2: Schematic illustration of the semiconductor materials when used for degradation contaminants in water under the sunlight.

$$\text{Semiconductor (SC)} + h\upsilon \rightarrow \text{SC}(e^- + h^+) \quad \textbf{(2.1)}$$

$$\text{SC } e^- + O_2 \rightarrow \text{SC} + O_2^- \quad \textbf{(2.2)}$$

$$O_2^- + H_2O \rightarrow \text{SC} + \cdot OH \quad \textbf{(2.3)}$$

$$\text{SC}(h^+) + OH^- \rightarrow \text{SC} + \cdot OH \quad \textbf{(2.4)}$$

As a result of consecutive reaction highly reactive peroxide (O_2^-) and hydroxyl radical (·OH) attack the organic contaminants (OCs) on the surface leading to degradation.

$$\text{OCs} + \cdot OH \rightarrow CO_2 + H_2O \quad \textbf{(2.5)}$$

Thus optically illuminated photocatalyst semiconductor can degrade and mineralize organic compounds through a series of oxidation reactions.

2.1.2. Titanium dioxide

The element Titanium was discovered in 1791 by William Gregor, in England. Martin H. Klaproth was not able to make the pure element of titanium however he was only able to produce titanium dioxide (TiO_2). TiO_2 is a multifaceted compound. It's the stuff that makes toothpaste white and paint opaque. TiO_2 is also a potent photocatalyst that can break down almost any organic compound when exposed to sunlight, and a number of companies are seeking to capitalize on TiO_2's reactivity by developing a wide range of environmentally beneficial products, including self-cleaning fabrics, auto body finishes, and ceramic tiles. TiO_2 as a photocatalyst for purification of waste water have grown significantly since the discovery of

photocatalytic water splitting on TiO_2 by Fujishima and Honda in 1972 [6]. Titanium dioxide has long been regarded as an attractive photocatalyst, however, the use of titanium dioxide is impaired by its wide band gap (3.2-3.6 eV) [37],which requires ultraviolet (UV) irradiation for photocatalytic activation (λ <387 nm). As known, UV light accounts for only about 5 % of solar energy while visible light does 45 % [38]. The shift of the optical response of titanium dioxide from UV to the visible spectral range will have a profound positive effect on the efficient use of solar energy in photocatalytic reactions. Therefore, considerable efforts have focused on band-gap engineering of TiO_2 by incorporating several atoms in to structure.Titanium dioxide is a well-known photocatalyst for water and air treatment as well as for catalytic production of gases. The general scheme for the photocatalytic destruction of organics begins with its excitation by supra bandgap photons, and continues through redox reactions where OH radicals, formed on the photocatalyst surface, play a major role. Titanium dioxide is non-toxic and therefore is used in cosmetic products (sunscreens, lipsticks, body powder, soap, pearl essence pigments, tooth pastes) and also in special pharmaceutics. Titanium dioxide is even used in food stuffs, for instance in the wrapping of salami. Small amounts added to cigar tobacco are the cause of the white ash cigar smokers so cherish.

Titanium dioxide has three different main crystal structures; rutile (tetragonal, a=b=4.584 Å, c=2.953Å), anatase (tetragonal, a=b=3.782 Å, c=9.502 Å) and brookite (orthorhombic, a=9.166 Å, b=5.436 Å, c=5.135 Å) [71]. The two commonly available stable phases of TiO_2 are rutile and anatase. These phases transitions begins to appear at 280-480^oC, 480-880^oC for anatase phases and rutile phases, respectively [72]. Rutile structure is more stable about 1.2-2.8 kcal/mol than anatase structure. Rutile is preferred to anatase for optical and dielectric applications because of its high refractive index and dielectricity. Whereas, anatase is preferred for all applications related to photocatalytic activity due to its higher charge carrier mobility. The anatase phase is like pyramid structure and, it is stable at low temperatures. The crystals of rutile phase are needle-shaped structure and, this phase is formed at elevated temperatures. Both of rutile and anatase phases are used mostly as compared with brookite phase. The crystal lattice structures of rutile, anatase and brookite phases are showed in Figure 2.3.

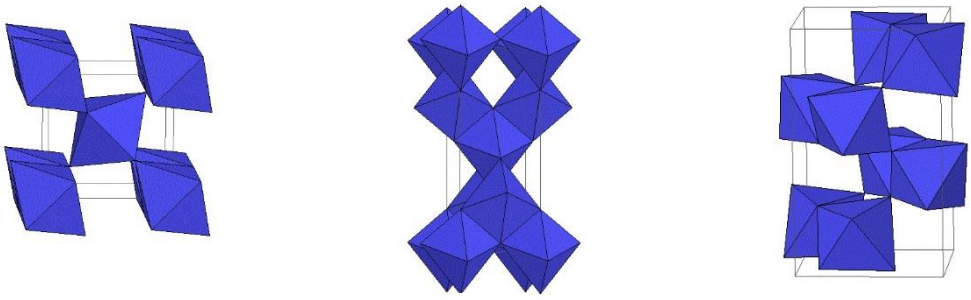

a b c

Figure 2.3: Representation of the crystal lattice structures of TiO_2 phases; a) rutile, b) anatase, c) brookite [71].

Titanium dioxide is an n-type semiconductor having a band gap of 3.2 and 3.6 eV, respectively, for anatase and rutile phases. Electronic structure of TiO_2 has been determined experimentally by various groups [73]. The valence bands of TiO_2 can be split into three main regions: the σ bonding in the lower energy region mainly due to O-p σ bonds; the π bonding in the middle energy region; and O-p π states in the higher energy region due to O-p π nonbonding states where the hybridization with d states of titanium is almost negligible. The conduction band is split into titanium eg (>5 eV) and t2g bands (<5 eV). The d_{xy} states of t2g are dominantly located at the bottom of the conduction band. The rest of the t2g bands are anti-bonding with p states of oxygen. The main peaks of the t2g bands are identified to be constituted by mostly d_{yz} and d_{zx} states. The lowest empty energy levels are titanium d_{xy} and thus they are representative of the conduction band (CB) edge, whereas full O p states define the valence band (VB). The conductivity of TiO_2 is mainly dependent upon the presence of oxygen vacancies and Ti^{3+} cations, which makes TiO_2 an n-type semiconductor. Key point of the optical and electrical properties is the presence of defects that provide additional states in the bandgap near the CB or VB. When the semiconductor TiO_2 absorbs photons with energy equal to or greater than its Eg, the electrons in VB will be excited to CB, leaving the holes in VB. This electron−hole pair generation process in TiO_2 can be expressed as follows:

$$TiO_2 + h\upsilon \rightarrow e^- (TiO_2) + h^+ (TiO_2) \quad \textbf{(2.6)}$$

In literature, there are various works about doping in titanium dioxide as listed in Table 2.1. Macak et al reported nitrogen (N) doping of self-organized titanium dioxide nano-tubular layers in 2006 [39]. After year, Li et al doped copper (Cu) in titanium dioxide nanotube array [53], Yang et al studied at co-doping with carbon (C) and vanadium (V) of titanium dioxide nanotube arrays [52], and Chen et al tried

to make carbon (C) and nitrogen (N) co-doped titanium dioxide and reported N atoms could incorporate into the lattice of anatase through substituting the sites of oxygen atoms, while most C atoms could form complex carbonate species at the surface of titanium dioxide nanoparticles [74]. In 2008, Su et al doped boron in titanium dioxide nanotube array and Zhang et al demonstrated the synthesis of P-doped TiO_2 NTs with uniform [41, 55]. In recent years, tungsten (W) and nitrogen (N) co-doped titanium dioxide nanotube arrays, molybdenum (Mo) and nitrogen co-doped titanium dioxide nanotube arrays, silver (Ag) doped titanium dioxide nano-materials, and in addition to these, molybdenum, antimon (Sb) and sulphide (S) tridoped titanium dioxide nano-particles were fabricated by researchers [38, 42, 49, 51].

Table 2.1: Some studies in literature based on doped titanium dioxide.

Dopant	Materials' Form	Method	Referance
W-N	Film on titanium sheets	Anodization/ Hydrothermal	Min Zhang, et al. 2013 [38]
N	Film on titanium foil	Anodization/Heat treatment	J.M. Macak, et al. 2006 [39]
P	Film on titanium foil	Anodization	Yanyan Zhang, et al. 2008 [41]
Mo–Sb–S	Powder	Sol-gel	Deliang Li, et al. 2014 [42]
Mo-N	Film on titanium sheets	Anodization/ Hydrothermal	Min Zhang, et al. 2013 [49]
N-V	Film on titanium foil	Anodization/ Hydrothermal	Jiasong Zhong, et al. 2014 [50]
Ag	Powder	Sol-gel	X.F. Lei, et al. 2014 [51]
C-V	Powder	Sol-gel	Xiangxin Yang, et al. 2007 [52]
Cu	Powder	Sol-gel	Haibin Li, et al. 2007 [53]
B	Film on titanium sheets	Anodization/CVD	Yaling Su, et al. 2008 [55]
C-N	Powder	Sol-gel	Daimei Chen, et al. 2007 [74]

2.2. Electrochemical Anodization

2.2.1. Basics of anodization

Anodization is an electrochemical passivation process, which is applied to some metallic materials (Ti, Zn, Al and etc.) having their own natural oxide layers. As in all electrochemical interactions, reduction and oxidation (redox) reactions also occur in anodization processes. Redox reaction is a type of chemical interaction that involves a transfer of electrons between two species. Since all types of chemical bonding are related to electrons' motion, all of chemical reactions are fundamentally electrical interactions. In addition to that, electrochemical studies provide to understand and make systematic to redox reactions. A schematic anodization cell in which these reactions take place is illustrated in Figure 3.1.

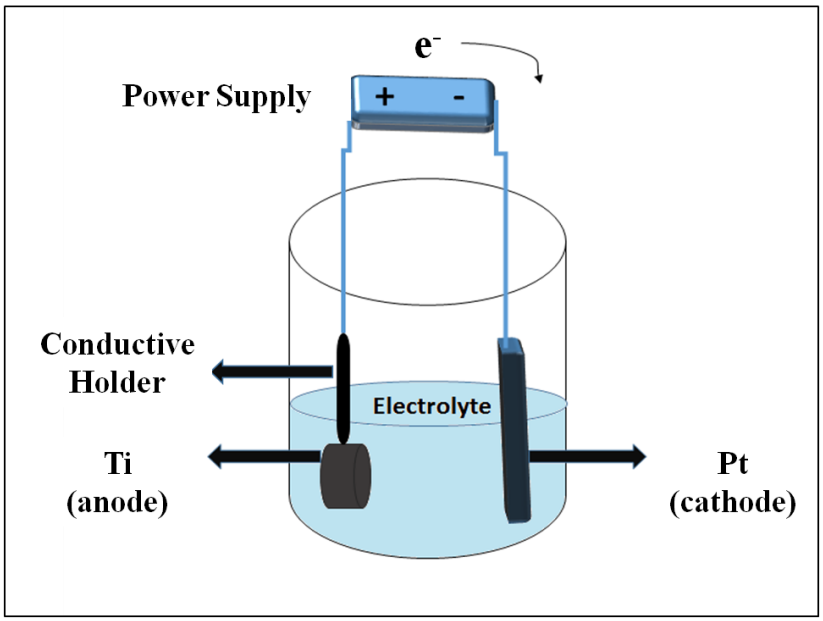

Figure 2.4 : Schematic illustration of anodization process

Basically, an electrochemical process is indicated by anode and cathode reactions as follows;

Anode: $2H_2O \rightarrow O_{2(g)} + 4H^+ + 4e^-$ **(3.1)**

Cathode: $2e^- + 2H_2O \rightarrow H_{2(g)} + 2OH^-$ **(3.2)**

However, anode reaction of the anodization process forms metal oxide on the metal surface through electrolysis. When metal are exposed to a adequately anodic voltage in an electrolytic cell (as in Figure 3.1.a), an oxidation reaction $M \rightarrow M^{x+} + xe^-$ will

be started. On the basis of electrolyte and specific anodization parameters, constitutively three possibility states: I) The M^{x+} ions are solvated in the electrolyte; II) the M^{x+} ions react with oxygen ions (O^{2-}) which provided by H_2O in the electrolyte and form an ordered oxide (MO) layer if MO is not solvable in the electrolyte; III) under some electrochemical conditions, both solvation and oxide formation get into competition leading to porous MO [75]. Under determined experimental conditions, growth of porous oxide can take place [76]. Furthermore, under some specific conditions, growth of TiO_2 nanotube arrays or formation of thick self-organized mesoporous layers can be observed [33-36, 77].

2.2.2. Anodization of titanium

Anodization of titanium is an electrolytic process that creates a protective or decorative oxide film over a metallic titanium surface. Anodization typically increases both the thickness and density of the oxide layer that forms on metal surface exposed to ambient conditions. In order that, the metallic titanium is connected to the positive terminal of a direct current power supply and placed in an electrolytic bath where it serves as the anode (as in Figure 2.1). The cathode is commonly a plate or rod of platinum, although materials such as carbon are sometimes used. In the process, migration of electrons occurs, but is also necessary for oxygen ions (O^{2-}) and M^{2+} ions to be combined. Basically, at the interface; oxygen atoms add two electrons to become oxide ions, at the surface of the metal; metal atoms are oxidized to metal ion by losing electrons. When power (electrical potential) is applied, electrons are forced from the electrolyte to the positive anode. It provides to leaved surface metal atoms exposed to oxygen ions (O^{2-}) within the electrolyte. The atoms react and become an in situ integral part of the oxide layer. The electrons travel through the power source and return to the cathode where, if an appropriate electrolyte pH is present, they react with hydrogen ions and the combination bubbles off as hydrogen gas. Since the metal oxide partially dissolves in any electrolyte, it is necessary to use only those electrolytes for which the oxide forms more rapidly than it dissolves. The electrolyte composition is important for the production of either porous oxide surface or flat barrier oxide surface. Oxide barrier layers grow in those neutral or slightly alkaline solutions in which titanium dioxide is generally insoluble. Porous oxide layers grow in acidic electrolytes with fluoride [76]

in which oxide forms rapidly dissolves without current supplying. The acid cations also affect the resulting nanotube array structures. Fabrication of TNTAs via anodic oxidation of Ti was first reported in 2001, and later studies focused on accurate control and extension of the nanotube morphology, length and pore size, and wall thickness [78].

TiO_2 nanotube arrays synthesis can be made by using aqueous, buffered, polar organic or non-fluorid based electrolytes [78]. In literature, used aqueous electrolytes; these are HF (hydrofluoric acid), HNO_3/HF (nitric acid/hydrofluoric acid mix), H_2SO_4/HF (sulfuric acid/hydrofluoric acid mix), $H_2Cr_2O_7$/HF (dichromic acid/hydrofluoric acid mix), CH_3COOH/NH_4F (acetic acid/ammonium fluoride mix), H_2SO_4/NH_4F (sulfuric acid/ammonium flouride mix), H_3PO_4/HF (phosphoric acid/hydrofluoric acid mix), H_3PO_4/NH_4F (phosphoric acid/hydrofluoric acid mix) containing electrolytes. As an example of buffered electrolytes are KF (potassium fluoride) or NaF (sodium fluoride) / NaOH (sodium hydroxide) / H_2SO_4, $NaHSO_4$ (sulfuric acid, sodium hydrogen sulphate) or $C_6H_8O_7$ (citric acid) containing solutions. Species of electrolytes; these are formamide (CH_3NO), dimethly formamide (C_3H_7NO), dimethly sulfoxide (C_2H_6OS;DMSO), ethylene glycol ($C_2H_6O_2$), diethylene glycol ($C_4H_{10}O_3$), methanol/water/hyrogenfluoride (CH_4/H_2O/HF) electrolytes used to produce formation of longer nanotubes [60]. In addition to these, non-fluoride based electrolytes are used for TNTAs. By using titanium foil as anode and copper as cathode in HCl (hydrogen chloride) electrolyte solutions, TNTAs were formed [61]. Another electrolyte is consist of H_2O_2 (hydrogen peroxide) aqueous or HCl/ H_2O_2 solution [79].

Mechanism of TNTAs formation by anodization is clarified by key points of the process that are: (1) oxide growth at the metal surface due to interaction of the metal with O^{2-} or OH^-ions. After formation of an initial oxide layer, these anions migrate through the oxide layer reaching the metal/oxide interface where they react with the metal. (2) Metal ion (Ti^{4+}) migration from the metal at the metal/oxide interface; Ti^{4+} cations will be discharged from the metal/oxide interface under application of an electric field that move toward the oxide/electrolyte interface. (3) Due to the applied electric field the Ti–O bond undergoes polarization and is weakened dissolution of the metal cations. Ti^{4+} cations dissolve into the electrolyte, and the free O^{2-} anions move to the metal/oxide interface, process (1), to interact with the metal.

(4) Chemical dissolution of the metal, or oxide, by the acidic electrolyte. Chemical dissolution of TiO_2 in the HF electrolyte and applying voltage play a critical role in the formation of nanotubes rather than simple nanoporous structures [79].

In the HF based aqueous electrolyte, reactions become as below;

$$4HF_{(aq)} \rightarrow 4H^{+}_{(aq)} + 4F^{-}_{(aq)} \quad \textbf{(3.3)}$$

$$4H_2O_{(aq)} \rightarrow 4H^{+}_{(aq)} + 4OH^{-}_{(aq)} \quad \textbf{(3.4)}$$

$$4F^{-}_{(aq)} + 4OH^{-}_{(aq)} \rightarrow 4O^{2-}_{(aq)} + 4HF_{(aq)} \quad \textbf{(3.5)}$$

$$Ti_{(s)} + 4H^{+}_{(aq)} + 4F^{-}_{(aq)} \rightarrow Ti^{4+}_{(aq)} + 4F^{-}_{(aq)} + 2H_{2(g)} \quad \textbf{(3.6)}$$

By the anodization started, the initial oxide layer formed due to interaction of the surface Ti^{4+} ions with oxygen ions (O^{2-}) in the electrolyte [79]. Reaction of oxide layer formation at the anode is as follows;

$$Ti^{4+}_{(aq)} + O^{2-}_{(aq)} \rightarrow TiO_{2(s.c.)} \quad \textbf{(3.7)}$$

At the cathode, hydrogen gases occur as below reaction;

$$8H^{+}_{(aq)} + 8e^{-} \rightarrow 4H_{2(g)} \quad \textbf{(3.8)}$$

However, fluorine ions can attack the oxide layer if intensity of HF in the electrolyte is unnecessary, or the ions being mobile in the anodic layer under the applied electric field react with Ti^{4+} as follows;

$$TiO_{2(s.c.)} + 6F^{-} + 4H^{+} \rightarrow (TiF_6)^{2-}_{(aq)} + 2H_2O \quad \textbf{(3.9)}$$

$$Ti^{4+}_{(aq)} + 6F^{-} \rightarrow (TiF_6)^{2-}_{(aq)} \quad \textbf{(3.10)}$$

As a result of that, tetra fluoro titanate complex anions can be formed in electrolyte and it can be an obstacle to formation of nanotube arrays.

2.2.3. Doping into titanium dioxide nanotube layer by anodization

Semiconducting doping, namely band-gap engineering, is creating a secondary electronically active species into the lattice. The most typical methods to prepare doped TiO_2 nanostructures are: 1) treating growed TiO_2 nanomaterials in a solution or melt of the doping species; 2) thermal treatments in dopant rich gas atmospheres; 3) production of nanomaterials by sputtering in an atmosphere of dopant; 4) high-energy ion implantation; and 5) anodization in an electrolyte containing dopant solution [70].

In recent years, anodization processes have been used greatly to produce doped TiO_2 nanotube arrays. To accomplish it, different dopants as B (boron)[59], Nb (niobium) [80] added in fluoride based electrolyte.

In this study, B-doped TiO2 nanotube arrays were fabricated by anodization process according to below mechanism created by predicted possible electrochemical reactions;

$$HF_{(aq)} \rightarrow H^{+}_{(aq)} + F^{-}_{(aq)} \quad \textbf{(3.11)}$$

$$C_2O_4H_2.2H_2O_{(k)} + H_2O_{(aq)} \rightarrow C_2O_4^{2-}{}_{(aq)} + 5H^{+}_{(aq)} + 3OH^{-}_{(aq)} \quad \textbf{(3.12)}$$

$$NaBF_{4\,(aq)} + H_2O_{(aq)} \leftrightarrow Na^{+}_{(aq)} + BF_4^{-}{}_{(aq)} + H^{+}_{(aq)} + OH^{-}_{(aq)} \quad \textbf{(3.13)}$$

$$H_2O_{(aq)} \leftrightarrow H^{+}_{(aq)} + OH^{-}_{(aq)} \quad \textbf{(3.14)}$$

These reactions explain to components of electrolyte before apply current to anodization system. After apply current;

Anode reaction as follows,

$$F^{-}_{(aq)} + BF_4^{-}{}_{(aq)} + C_2O_4^{2-}{}_{(aq)} + OH^{-}_{(aq)} \leftrightarrow BF_{3(aq)} + C_2F_{6(aq)} + O_{2(g)} + O^{2-}_{(aq)} + H^{+}_{(aq)} + F^{-}_{(aq)} \quad \textbf{(3.15)}$$

$$Ti^{4+}_{(aq)} + O^{2-}_{(aq)} \rightarrow TiO_{2(s.c.)} \quad \textbf{(3.16)}$$

$$Ti^{3+}_{(aq)} + BF_4^{-}{}_{(aq)} + O^{2-}_{(aq)} \rightarrow TiBF_4O_{(s.c)} \quad \textbf{(3.17)}$$

$$Ti^{4+}_{(aq)} + B^{3+}_{(aq)} + O^{2-}_{(aq)} \rightarrow Ti\text{-}B\text{-}O \quad \textbf{(3.18)}$$

3. EXPERIMENTAL SECTION

3.1. Materials

Titanium (Grade 2, TiMET Metal & Medical Co.) cylinders with 15mm diameter and 10 mm thickness were used as substrates to form TNTAs.Hydrogen floride (HF, 40,0%, Sigma-Aldrich), oxalic acid dihydrate ($C_2O_4H_2.2H_2O$, ≥99,0% Sigma-Aldrich), nitric acid (HNO_3, ≥65% Sigma-Aldrich) sodium tetra-fluoro-borate ($NaBF_4$, 97,0+% Sigma-Aldrich), acetone (C_3H_6O, Sigma-Aldrich) and ethyl alcohol (C_2H_6O, Sigma-Aldrich) were used in production process of TNTAs. Methylene blue ($C_{16}H_{18}ClN_3S$, Sigma-Aldrich) was used for photocatalytic degradation tests. All of the chemicals were analytical grade and all experiments were carried out at room temperature using distilled water.

3.2. Method

3.2.1. Preparation of titanium substrates

The purchased 15mm diameter titanium rod was cut into cylinders as substrates with 10mm-height via sample cutting device (Struers, Lobotom 5). Subsequent to cutting process, substrates were sequentially grinded by 80-2000 grit emery papers. Grinded substrates were cleaned in acetone, ethyl alcohol and pure water containing solutions by an ultrasonic bath. Finally, the substrates with enhanced surfaces were obtained as seen in Figure 3. 1.

Figure 3.1: As grinded substrates

3.2.2. Fabrication and optimization of titanium dioxide nanotube arrays

In this study, fabrication of TNTAs were provided via electrochemical anodization in two different electrolytes defined as EH and EHOx. Electrolyte EH and EHOx included HF/H_2O and $C_2H_2O_4 \cdot 2H_2O/HF/H_2O$ respectively. Effects of anodization parameters (working voltages; V, processing times; t and HF concentrations; C) on surface morphologies of anodized structures were evaluated to determine optimum conditions for boron incorporation. The production flowchart for these processes is represented in Figure 3.2. According to the flowchart sample and code designation for anodization in EH and EHOx electrolytes were listed in table 3.1 and table 3.2 respectively. Herein, temperature for heat treatment was chosen according to literature [72].

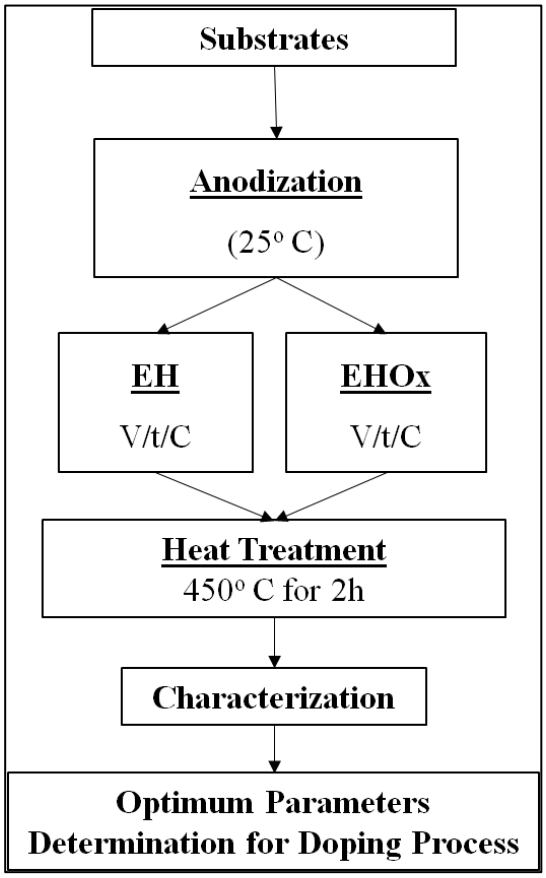

Figure 3.2: Flowchart of production and characterization of TNTAs.

Table 3.1: Samples anodized in EH.

Sample Code	Voltage	Time (min.)	HF (wt%)
V10t30C50	10V	30	0.50
V20t30C50	20V	30	0.50
V30t30C50	30V	30	0.50
V40t30C50	40V	30	0.50
V20t15C50	20V	15	0.50
V20t60C50	20V	60	0.50
V20t120C50	20V	120	0.50
V20t30C25	20V	30	0.25
V20t30C100	20V	30	0.10

Table 3.2: Samples anodized in EHOx.

Sample Code	Voltage	Time (min.)	HF (wt%)
Ox-V10t30C50	10V	30	0.50
Ox-V20t30C50	20V	30	0.50
Ox-V30t30C50	30V	30	0.50
Ox-V40t30C50	40V	30	0.50
Ox-V20t15C50	20V	15	0.50
Ox-V20t60C50	20V	60	0,50
Ox-V20t120C50	20V	120	0.50
Ox-V20t30C25	20V	30	0.25
Ox-V20t30C100	20V	30	0.10

The optimum anodization parameters were determined via SEM observations by determining the homogenous, smooth and uniform morphologies (see: 4.2.1. TiO_2 nanotube arrays) regarding to processing conditions.

3.2.3. Fabrication of boron doped titanium dioxide nanotube arrays

Based on the obtained results in prior anodization experiments, electrolytes EH and EHOx with optimized HF content were modified with sodium tetra fluoro borate as a chemical agent to provide boron incorporation. Hence the designations of the new electrolytes were defined as EHB and EHOxB to cite modified electrolytes EH and EHOx respectively. The contents of EHB and EHOxB consisted of $HF/H_2O/NaBF_4$ and $C_2H_2O_4 \cdot 2H_2O/HF/H_2O/NaBF_4$ respectively. Furthermore anodization processes were conducted with various concentrations of sodium tetra fluoro borate (0.015 and 0.030 wt% for EHB and 0.2, 0.5 and 1.0 wt % for EHOxB) for both electrolytes. Code-designations and processing parameters of the boron incorporated samples which were anodized in electrolytes EHB and EHOxB as listed in table 3.3 and table 3.4 respectively. Finally the samples were annealed at 450^oC for 2 hours in order to obtain crystalline anatase structure. Annealed samples were characterized with phase analysis (XRD), micro structural analysis (SEM/EDS/AFM), optical analysis (DRS) and photocatalytic test as outlined the flowchart in Figure 3.3.

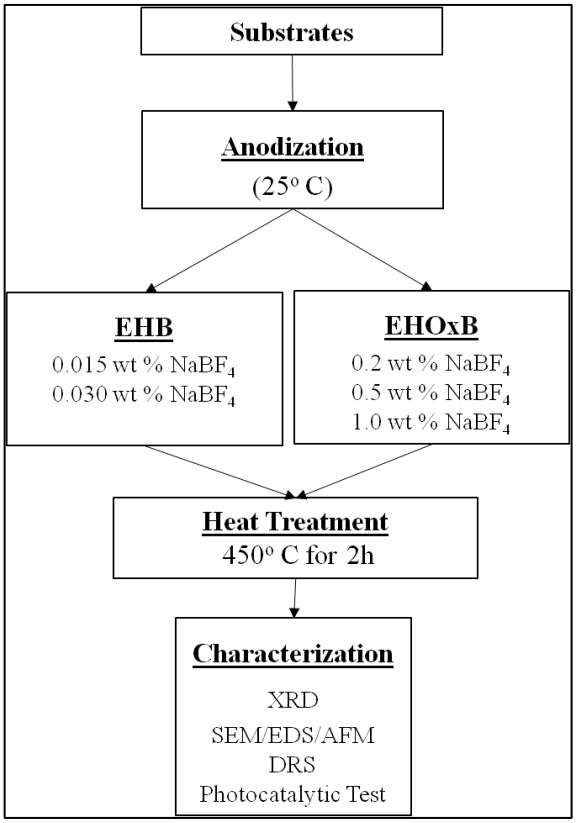

Figure 3.3: Flowchart of production and characterization of doped TNTAs.

Table 3.3: Samples anodized in EHB.

Sample Code	$NaBF_4$ Concentration (wt%)	Time (min.)	Voltage	HF (wt %)
B015-V20t120C50	0.015	120	20V	0.5
B030-V20t120C50	0.030	120	20V	0.5

Table 3.4: Samples anodized in EHOxB.

Sample Code	Dopant Concentration (wt %)	Time (min.)	Voltage	HF (wt %)
B2-Ox-V20t120C50	0.2	120	20V	0.5
B5-Ox-V20t120C50	0.5	120	20V	0.5
B10-Ox-V20t120C50	1.0	120	20V	0.5

3.2.4. Structural Characterization

X-ray diffraction (XRD) is one of the primary techniques to analyze all kinds of materials such as powders and crystals. XRD can provide information about crystalline structure and structural phases.

Measurements were performed by means of XRD with a grazing angle attachment and an incident angle of 1° (Rigaku, D/Max-2200/PC). X-Ray radiation of CuKα was set at 40 kV and 36 mA with a scanning speed of 4° 2θ/min, from 3° to 90°.

3.2.5. Morphological and Nanostructural Characterization

The Scanning Electron Microscope (SEM) is a versatile electron microscope that images a sample by scanning it with a high-energy beam of electrons in a raster scan pattern. In Typical SEM configuration, electrons are thermo ionic emitted from a tungsten or LaB6 cathode filament towards an anode. The electron beam, with a typical energy ranging from a few KeV to 30 KeV, is focused by successive lenses in a beam with a very fine spot size. When the beam introduces with the surface, different kind of electrons can be detected. The types of signals produced by an SEM include secondary electrons (SE), back-scattered electrons (BSE) and characteristic X-rays.

In this study, the surfaces of TiO_2/doped TiO_2 were examined by using JEOL JSM-7600F instrument operating at an accelerating voltage of 5.0 kV with several magnifications.

The atomic force microscope (AFM) is one kind of scanning probe microscopes (SPM). SPMs are designed to measure local properties, such as height, friction, magnetism, with a probe. To acquire an image, the SPM raster scans the probe over a small area of the sample, measuring the local property simultaneously. Using an atomic-force microscope (AFM), it is possible to measure a roughness of a sample surface at a high resolution, to distinguish a sample based on its mechanical properties (for example, hardness and roughness) and, in addition, to perform a micro fabrication of a sample (for example, an atomic manipulation). Figure 3.4 illustrates basically working princible of AFM.

In this study, 62,0x62,0 μm region at surfaces of doped TNTAs were scanned by using AFM (NanoSurf Flex AFM)operates with 256 lines.

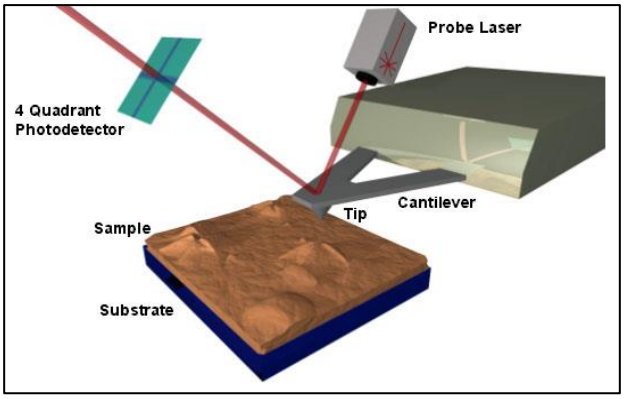

Figure 3.4: Typical configuration of AFM is illustrated [83].

3.2.6. Optical characterization

Optical characterization can be appointed by measuring of band gap energy. The measurement of the band gap of materials is important in the semiconductor and solar industries. The term “band gap” refers to the energy difference between the top of the valence band to the bottom of the conduction band; electrons are able to jump from one band to another. An electron is in need a specific minimum amount of energy to jump from a valence band to a conduction band. Mentioned energy is called the band gap energy. A diagram illustrating the bandgap is shown in Figure 3. 5.

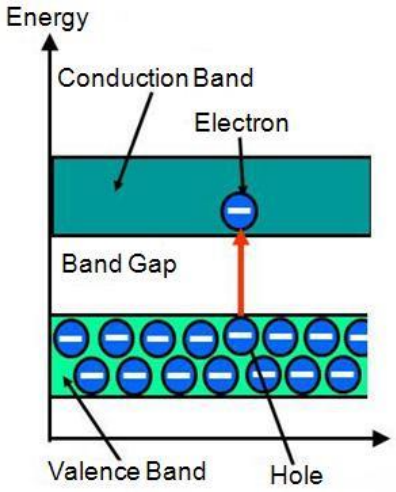

Figure 3.5: Schematic illustration of band [84].

The band gap energy can be calculated by equation is E=ħc/λ. Example of this calculation is given at table 3. 4. As a result of this calculations, equation is Eq**. (3.1)** $E = 1240/\lambda$ find directly to band gap energy value [85, 86]. Value of λ is cut off wavelength value which can be determined by wavelength to absorbance diagram from diffuse reflectance spectroscopy (DRS). Principle of DRS is schematized in Figure 3.6.

Table 3.5: Calculations of band gap energy [85, 86].

Band Gap Energy (E) = h*c/λ				
ħ= Planks constant = 6.626 x 10^{-34} Joules sec				
c = Speed of light = 3.0 x 108 meter/sec				
λ = Cut off wavelength = 410.57 x 10^{-9} meters				
ħ	c	λ	E	eV
6.63E-34	3.00E+08	4.11E-07	4.84156E-19	3.025976
Where 1eV = 1.6 X 10^{-19} Joules (conversion factor)				

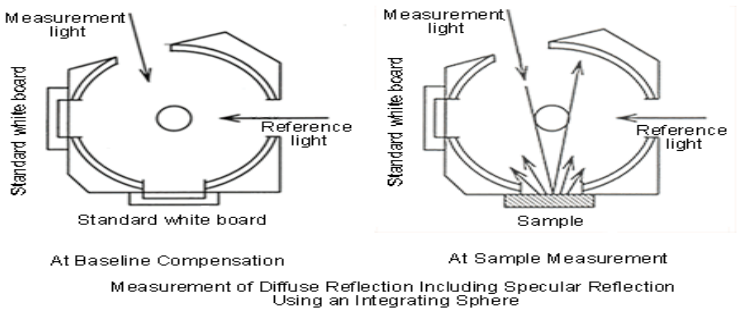

Figure 3.6: Illustration of DRS principle [87].

In this study, reflectance of undoped samples and doped samples were measured by Evolution 600 UV-Vis Thermo Scientific DRS device. Values of reflectance were converted by program driving to DRS device. The wavelength absorbance diagrams of these samples were drawn and the cut off wavelength was determined for all samples, therefore, the band gap energy was calculated accordingly mentioned calculations.

3.2.7. Photocatalytical Characterization

Aqueous methylene blue (MB) solutions are mostly employed artificial impurities in literature so as to evaluate the photocatalytic activity of the catalysts [38, 42, 46, 74, 76, 81, 84]. MB was first prepared in 1876 by German chemist Heinrich Caro from methyl-aniline. Methylene blue is an organic compound which is heterocyclic aromatic with the chemical formula $C_{16}H_{18}N_3SCl$. MB aqueous solution (MB^+) is a cationic dye with maximum absorption of light around 664 nm [88]. With this manner, to determine the photocatalytic degradation performance and kinetics of the TNTAs, Lambert-Beer correlation curve is plotted, and a linear relation between absorbance (A) and concentration (C) is identified by this way [89].

Lambert-Beer correlation curve is derived by Lambert-Beer equation which is expressed as; Eq. **(3.2)** $A = Absorbance = \log I0 / I = \epsilon . L . C$. In the expression A, I_0, I, ϵ, L and C denote absorbency, initial light intensity, light intensity, coefficient of absorbency, light path and concentration respectively. This linear relationship between A and C is valid under some conditions; monochromatic ray, homogenous sample and < 0.01 molarity. In more concentrated solutions refractive index will increase and interaction of molecules will be effective (A-C the linear relationship is broken). As a result of these, the linear correlation curve was plotted through the samples with concentration 0 to $1x10^{-5}$M lower concentrated sample (Figure 3.7).

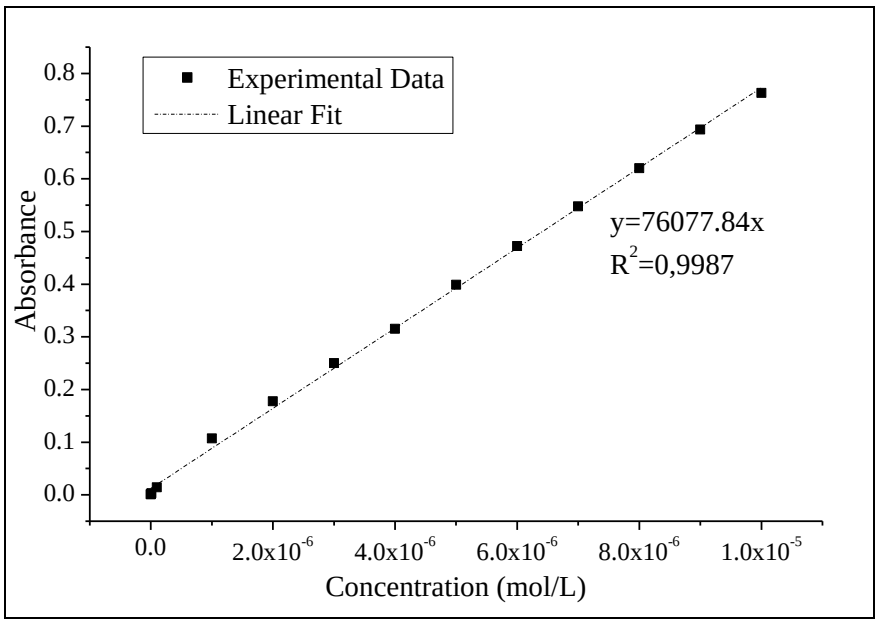

Figure 3.7: Absorbance-Concentration (mol/L) correlation plot

Subsequent to derivation of the absorbance and concentration relation of aqueous MB solutions, the photocatalytical activity tests for both TNTA and B-TNTA samples were conducted by immersing samples in to beakers containing 25ml of $0.25x10^{-5}$ M methylene blue solutions. In order to record catalyst-free degradation of MB an arbitration solution was also prepared. The degradation reactions were performed by exposing the samples to the UV irradiation with a light source (Osram Uv Vitalux 300 W/m^2) in a photocatalytic reactor depicted in Figure 3.8. To prevent the evaporation of the MB solutions, a transparent glass cap was placed above the beaker and water cooling system was used around the beakers (Figure 3.8). The degradation efficiencies are calculated by using absorbance values at 664nm obtained from UV-Vis spectrophotometer (UV mini-1240 UV-Vis/Shimadzu) in different intervals.

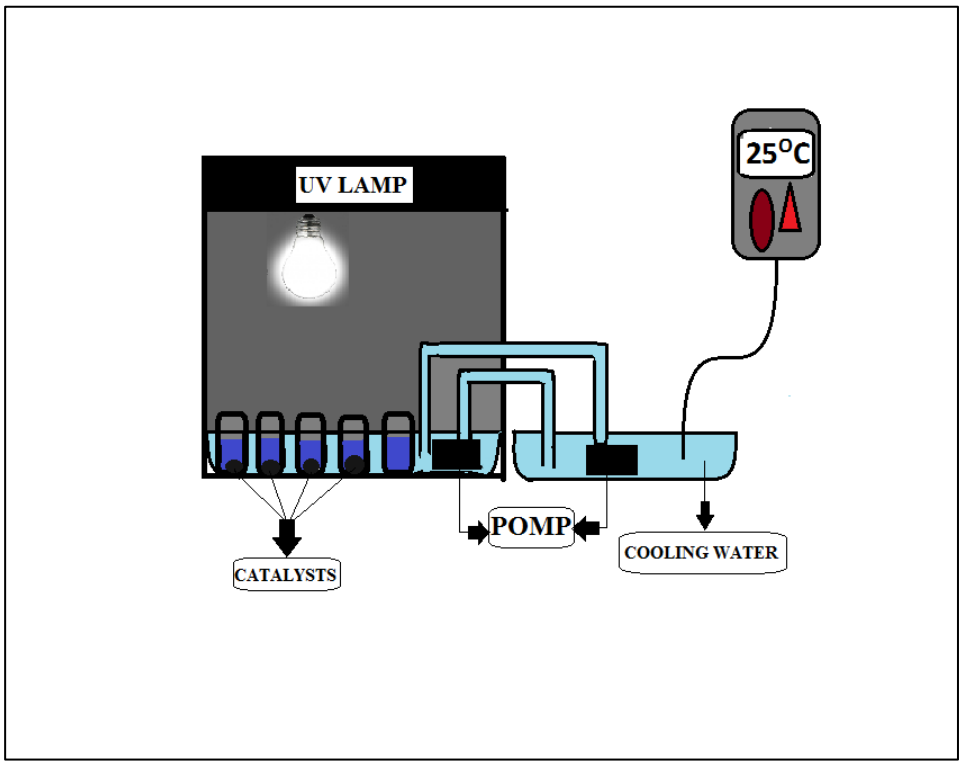

Figure 3.8: System of UV simulator and photocatalytic experiment setup illustrated schematically.

Furthermore the recorded absorbencies of the samples were converted to concentrations for different intervals. Using the concentrations, the degradation efficiencies and the reaction kinetics of the samples were calculated, in order to point out the effect of boron incorporation on the photocatalytical properties of the TNTA.

4. RESULTS AND DISCUSSION

Production and characterization of titanium dioxide nanotube structures and boron incorporation studies were sequentially performed in this research. Therefore, in this section of the thesis; phase structure, nanostructure, surface morphology, band gap measurements and photocatalytical properties of the samples will be presented in accordance with literature.

4.1. Phase Analysis

Crystalline structure and phases of the samples were determined by examining the x-ray diffraction patterns. The XRD patterns of the samples anodized in electrolyte EHB (V20T120C50, B125-V20T120C50, B25-V20T120C50) and EHOxB (Ox-V20T120C50, B2-Ox-V20T120C50, B5-Ox-V20T120C50, B10-Ox-V20T120C50) were represented in Figure 4.1 and Figure 4.2, respectively. According to the results it can be stated that all of the patterns are including two crystalline phases. These phases are anatase TiO_2 (JCPDS 021-1272) and titanium (JCPDS 044-1294) which belong to TNTAs and titanium substrates, respectively. Dominant diffraction peaks at $2\theta = 35^o$, 40^o correspond to metallic titanium substrate for all samples. Other characteristic peaks at $2\theta = 25.2^o$; 37^o; 37.9^o and 38.5^o were observed for both TNTA and B-TNTA structure corresponding to anatase TiO_2. It can be inferred that; as a result of the sequental anodization and heat treatment, production of photocatalytically active anatase phase was succesfuly obtained for all samples. In addition, it can be expressed the intense peaks of titanium substrates were obtained owing to low thicknesses of anodized layers. Since the diffraction characteristics are similar for all samples, patterns for the samples anodized in EH and EHOx (except V20T120C50 and Ox-V20T120C50) was not presented in this title.

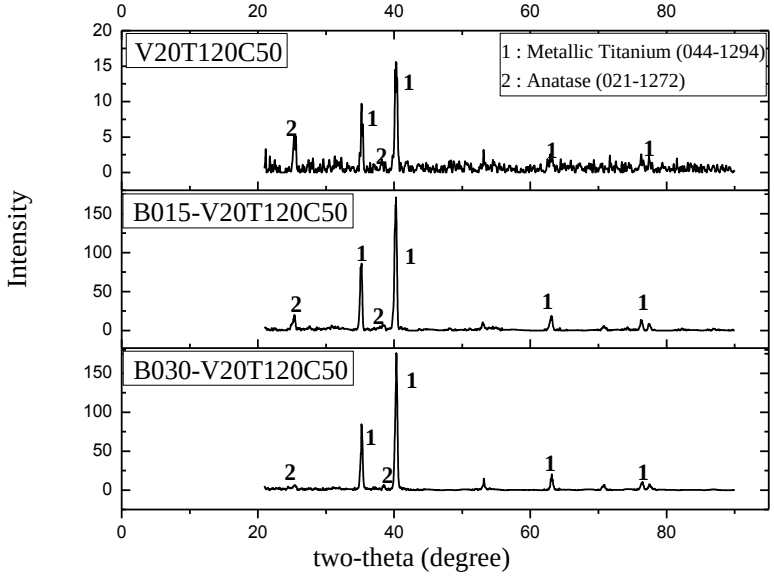

Figure 4.1: XRD patterns of the samples anodized in electrolyte EHB.

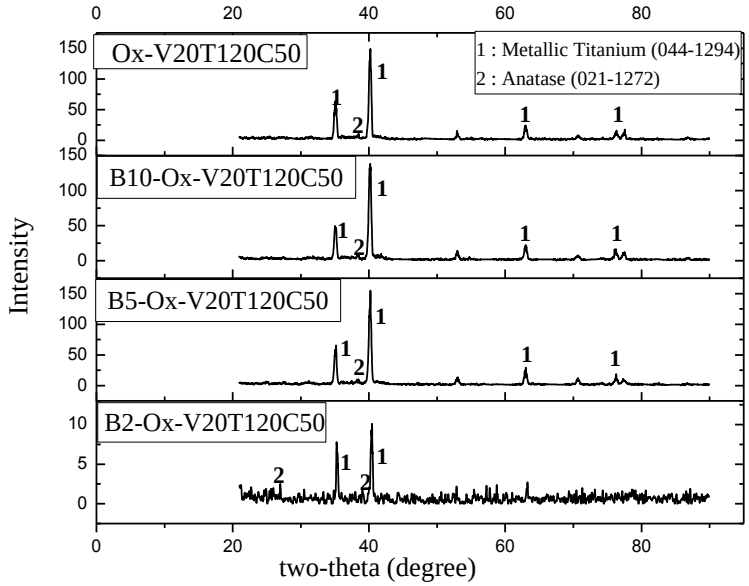

Figure 4.2: XRD patterns of the samples anodized in electrolyte EHOxB.

Obtained XRD patterns were found to be in a good agreement with the literature which are focused on the production of TNTAs [92-96]. In addition, it can be expressed that, obtained XRD results are similar with Na Lu [59] and Yaling Su [55, 58] who produced B-TNTA with different approaches. In addition any shift in the diffraction patterns were not observed as result of boron incorporation. As expressed by Na Lu [59] and Yaling Su [55, 58] the lower boron content make it hard to detect by XRD. Regarding to this, the boron contents in the structures were determined by energy-dispersive X-ray spectroscopy measurements in section 4.2.

4.2. Nanostructure Analysis

4.2.1. Titanium dioxide nanotube arrays

Surface morphology and structure of a catalyst is important for further photocatalytic tests. As mentioned elsewhere, the samples for the determination of optimum anodization parameters were produced in electrolyte EH and EHOx. The SEM images of these samples for various parameters were represented in Figure 4.3, 4.5, 4.7, and 4.4, 4.6, 4.8, for electrolyte EH and EHOx, respectively.

The SEM images of the samples anodized with anodization voltages 10V, 20V, 30V and 40V in electrolyte EH and electrolyte EHOx including 0.5wt% HF at 30 min were shown in Figure 4.3 and Figure 4.4. According to the figures, it can be expressed that formation of uniform and homogenously distributed TNTAs were occurred with sample anodized with 20V in electrolyte EH and EHOx.

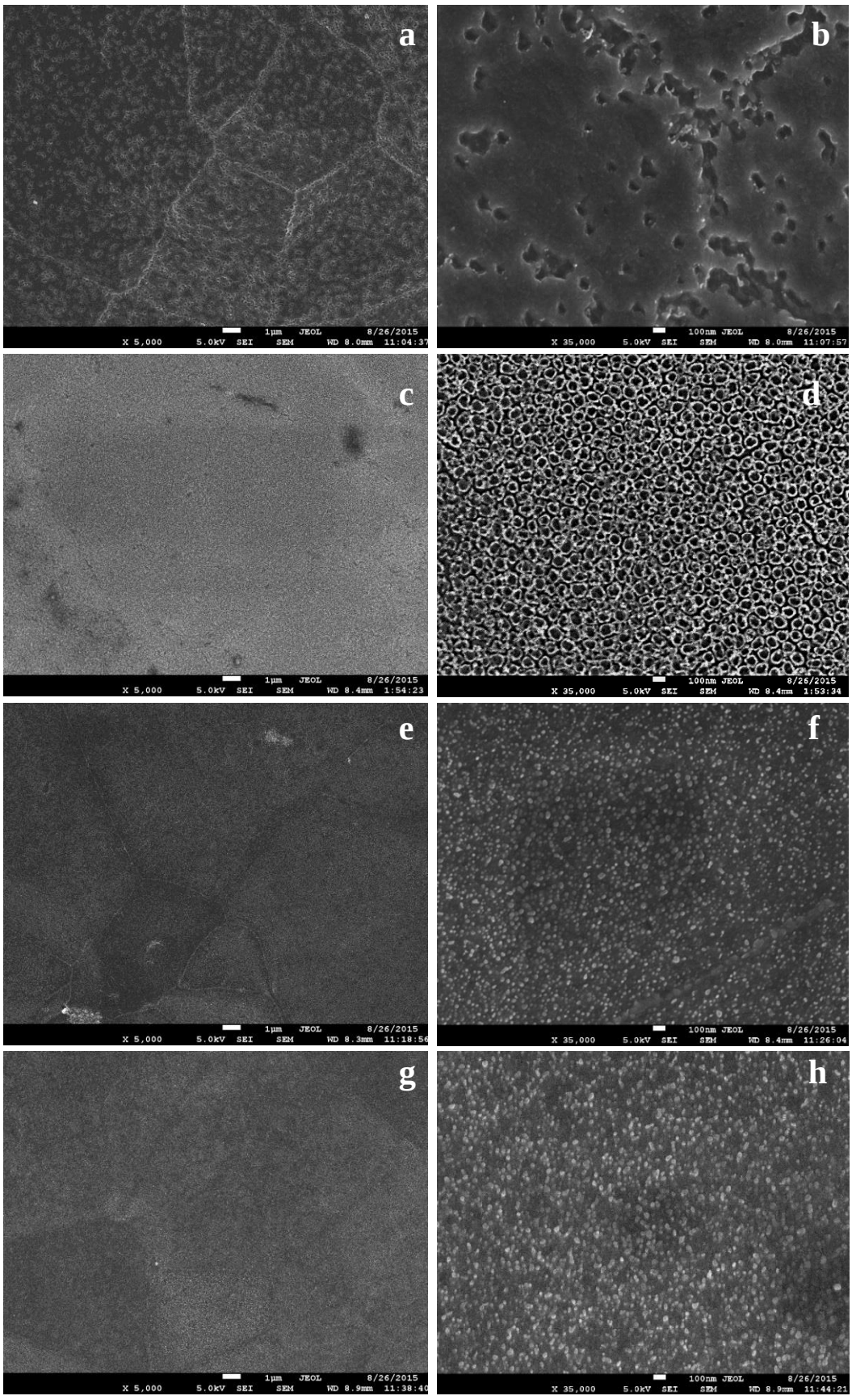

Figure 4.3: SEM images of samples produced in electrolyte EH including 0.5 wt% HF a, b) 10V, c, d) 20V, e, f) 30V, g, h) 40V.

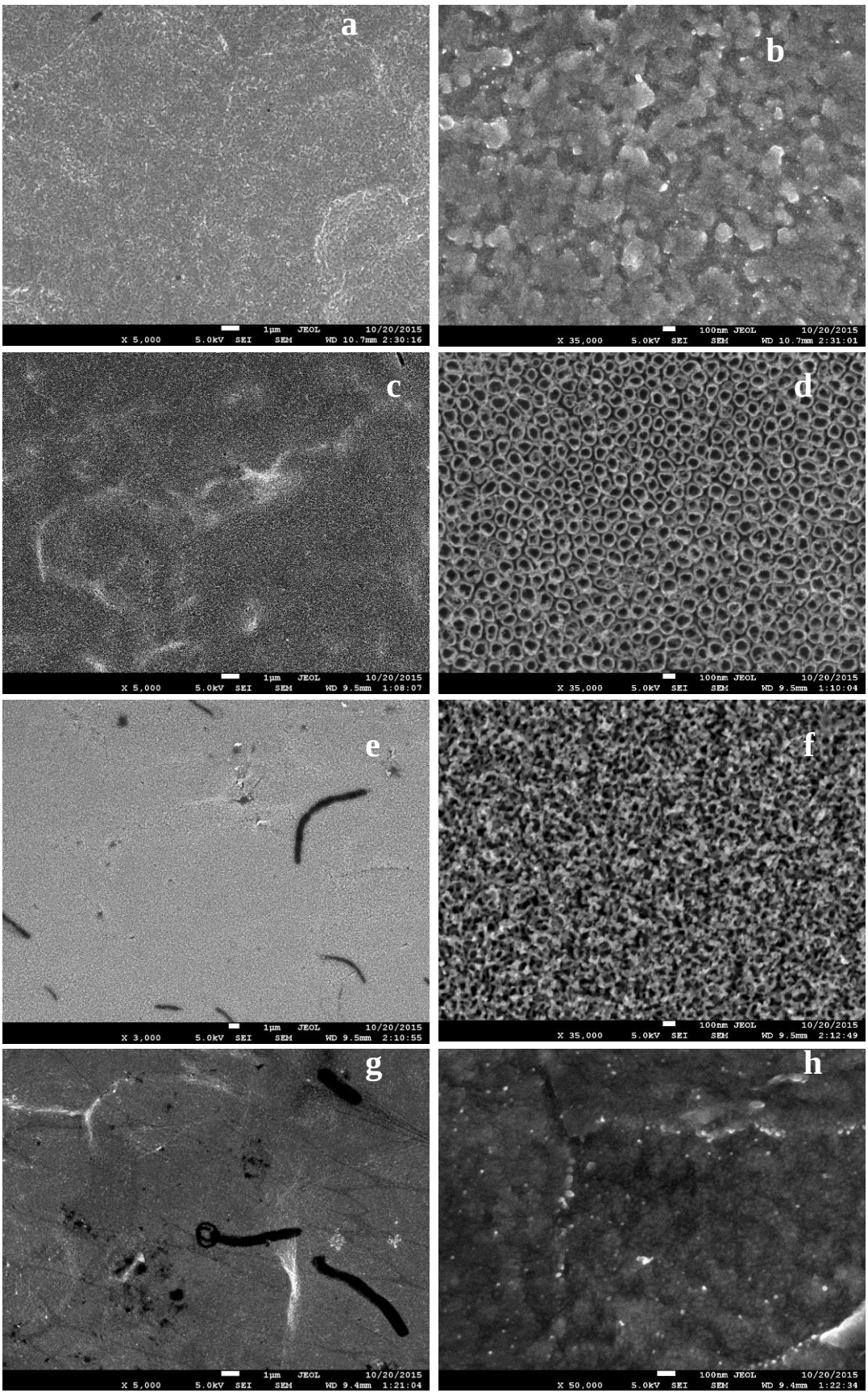

Figure 4.4: SEM images of samples produced in electrolyte EHOx including 0.5wt% HF. a, b) 10 V, c, d) 20 V, e, f) 30 V, g, h) 40 V.

In literature, Gong et al fabricated titanium dioxide nanotube arrays on titanium foil with voltages of 3, 5, 10 and 20V with anodizing time from 15-45 min. They observed that film morphology is nanoporous with pore sizes from 15 to 35 nm at low voltages. Discrete and cylindrical tube began to appear at voltages higher than 10V [29]. However, Erol et al reported a study about the effect of anodization parameters on the formation of nanoporous titanium dioxide layers. They worked to anodize at 20 ^{o}C for 30 min. at different voltages; 20, 30, 40, 50V and their results indicated that the formation of nanoporous structure was obtained by applying 20V similar to our results [81].

The SEM images of the samples anodized in electrolyte EH and EHOx including 0.25, 0.50 and 1.0 wt% HF with 20V at 30 min were shown in Figure 4.5 and Figure 4.6, respectively. According to the figures, it can be stated that uniform TNTAs were formed in both electrolyte EH and EHOx including 0.25 and 0.50 wt% HF.

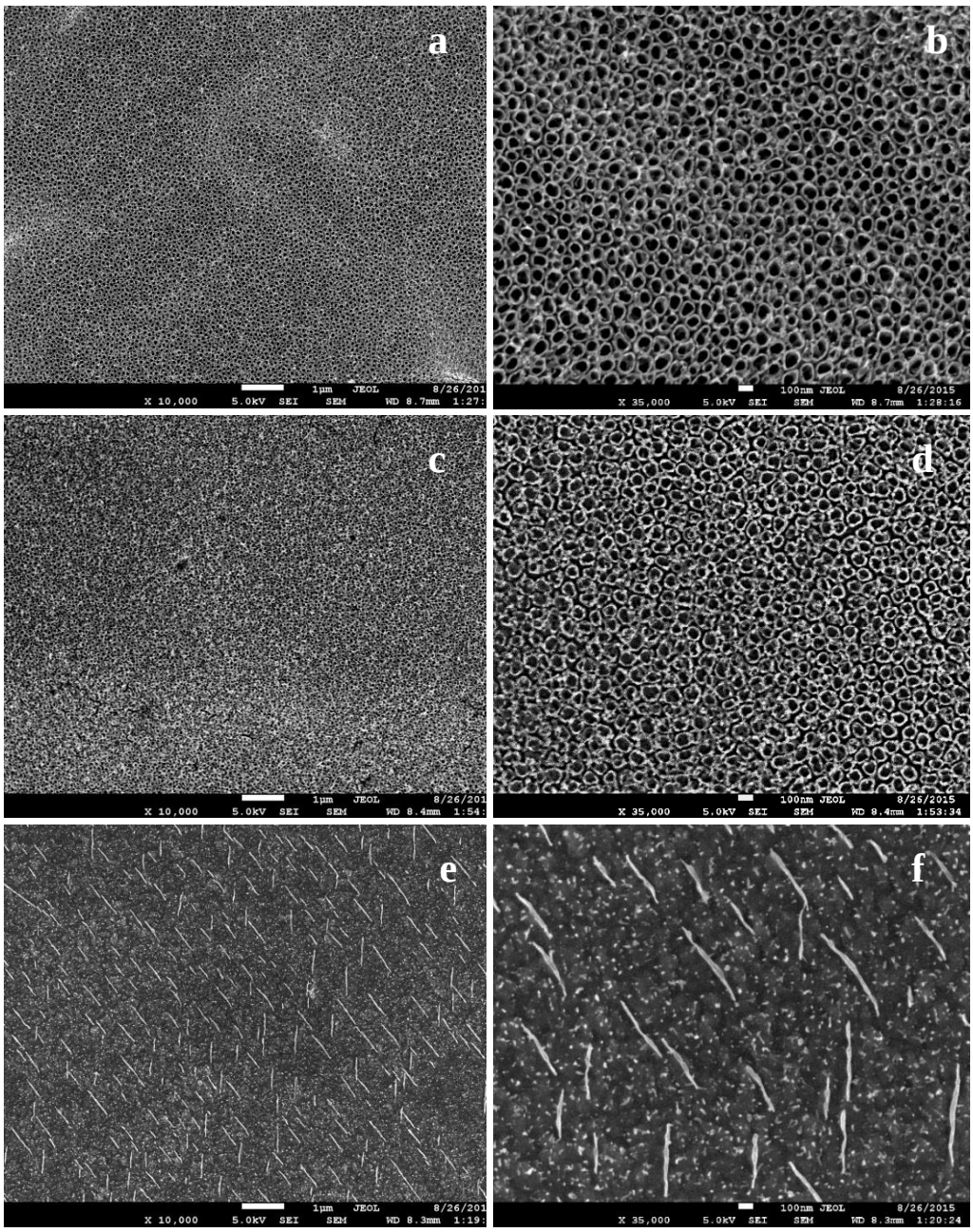

Figure 4.5: SEM images of samples produced in electrolyte EH with various HF content (wt%); a, b) 0.25; c, d) 0.5; e, f) 1,0 with 20V.

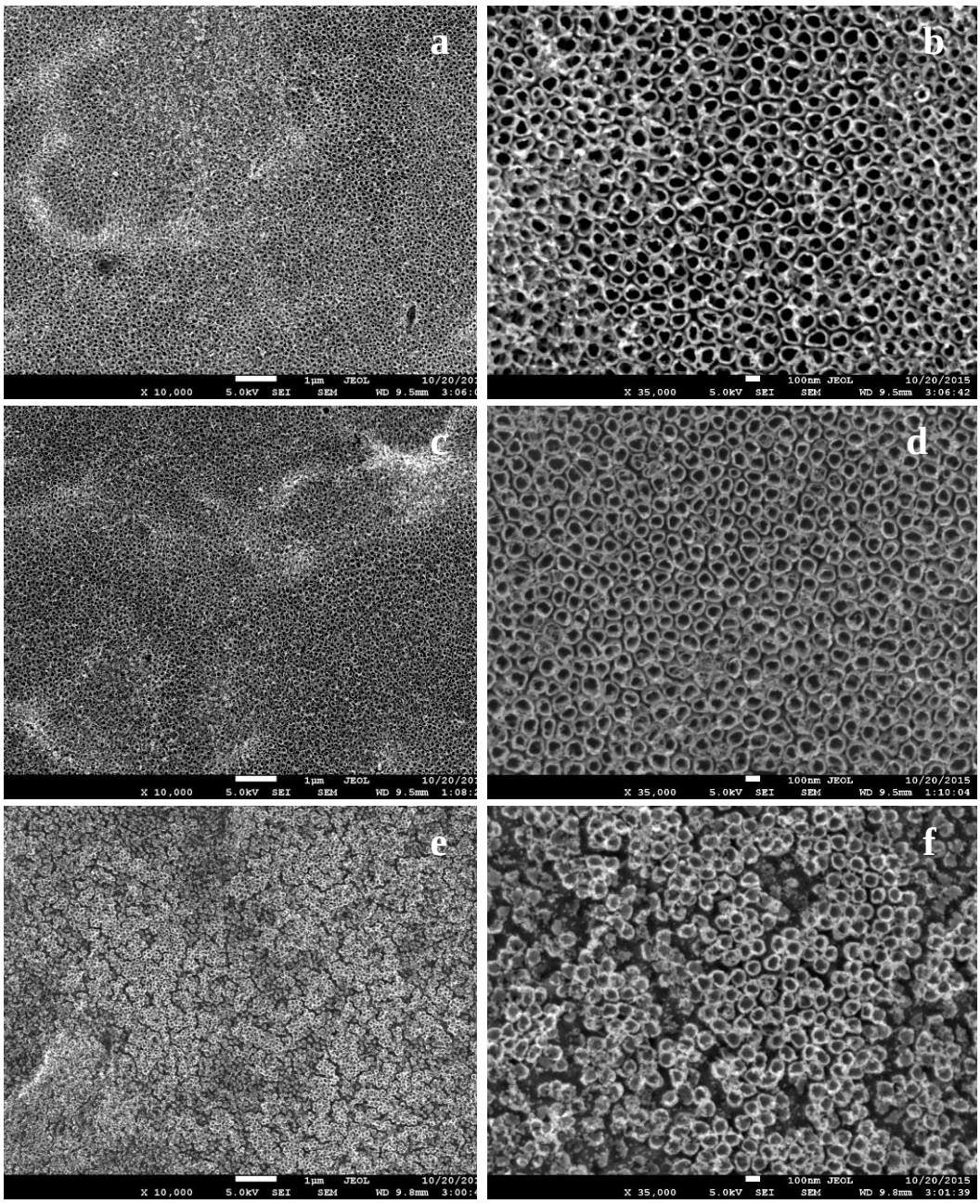

Figure 4.6: SEM images of samples produced in electrolyte EHOx with various HF content (wt%); a, b) 0.25; c, d) 0.5; e, f) 1,0 with 20V.

In literature, Dikici et al reported that they obtained titanium dioxide nano-pore by anodization process using 1.0 wt% HF electrolyte with applying 20V at 30 min [90]. However, in this study, we could not observe these structure as seen at SEM images (in Figure 4.5e,f) of sample produced by the similar conditions, using electrolyte EH. But the observation of the porous structures was provided with sample anodized in electrolyte EHOx including 1.0wt% HF according to SEM images in Figure 4.6 e, f.

The SEM images of sample produced in electrolyte EH and EHOx including 0.5wt% HF with 20V at 15, 30, 60, 120 min were shown in Figure 4.7 and Figure 4.8. According to Figure 4.7, formation of uniform TNTAs (samples anodized in electrolyte EH for 15, 30, 60 and 120 min) was obtained.

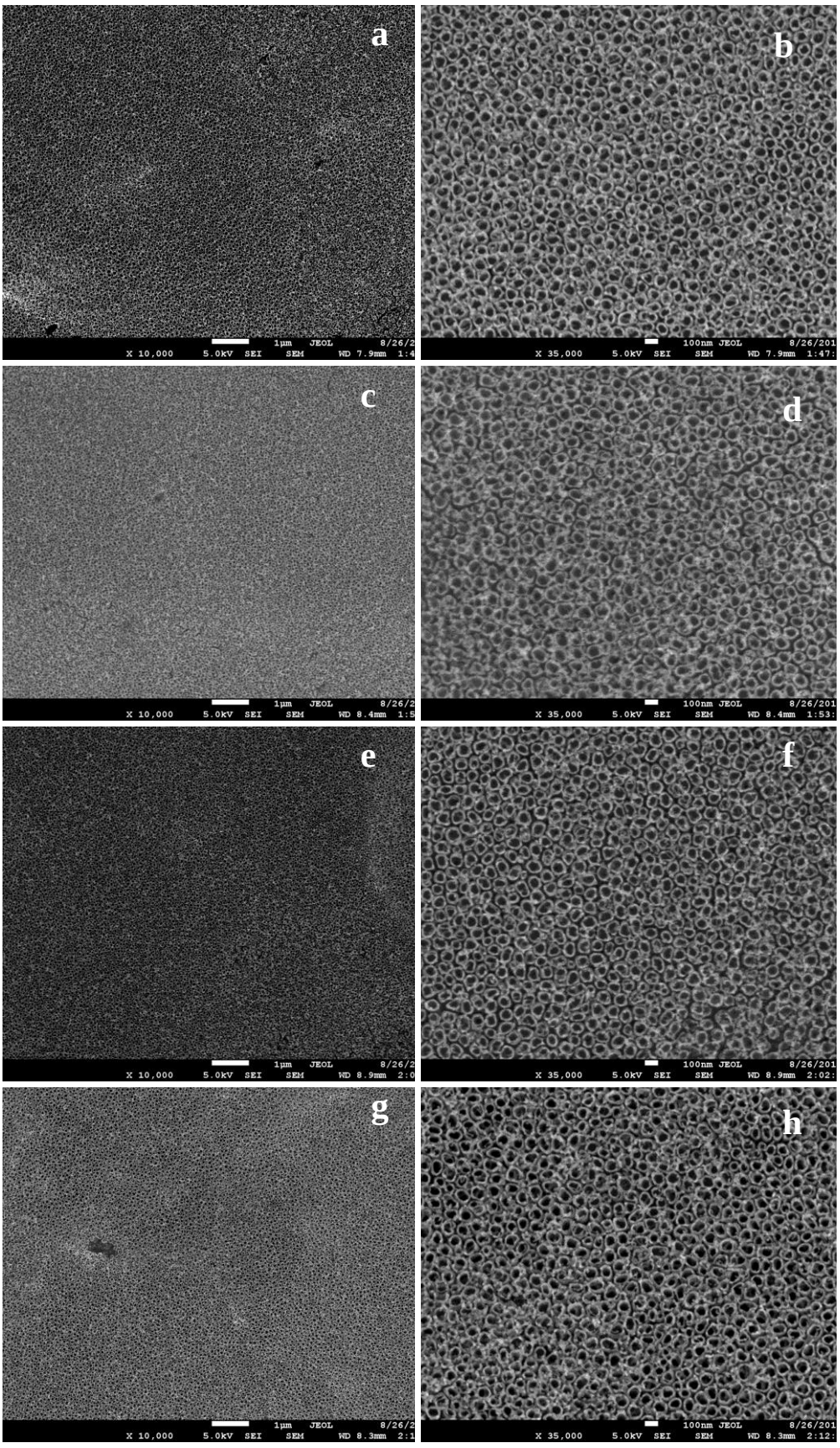

Figure 4.7: SEM images of samples produced in electrolyte EH including 0.5 wt% HF a, b) 15 min, c, d) 30 min, e, f) 60 min, g, h) 120 min with 20V.

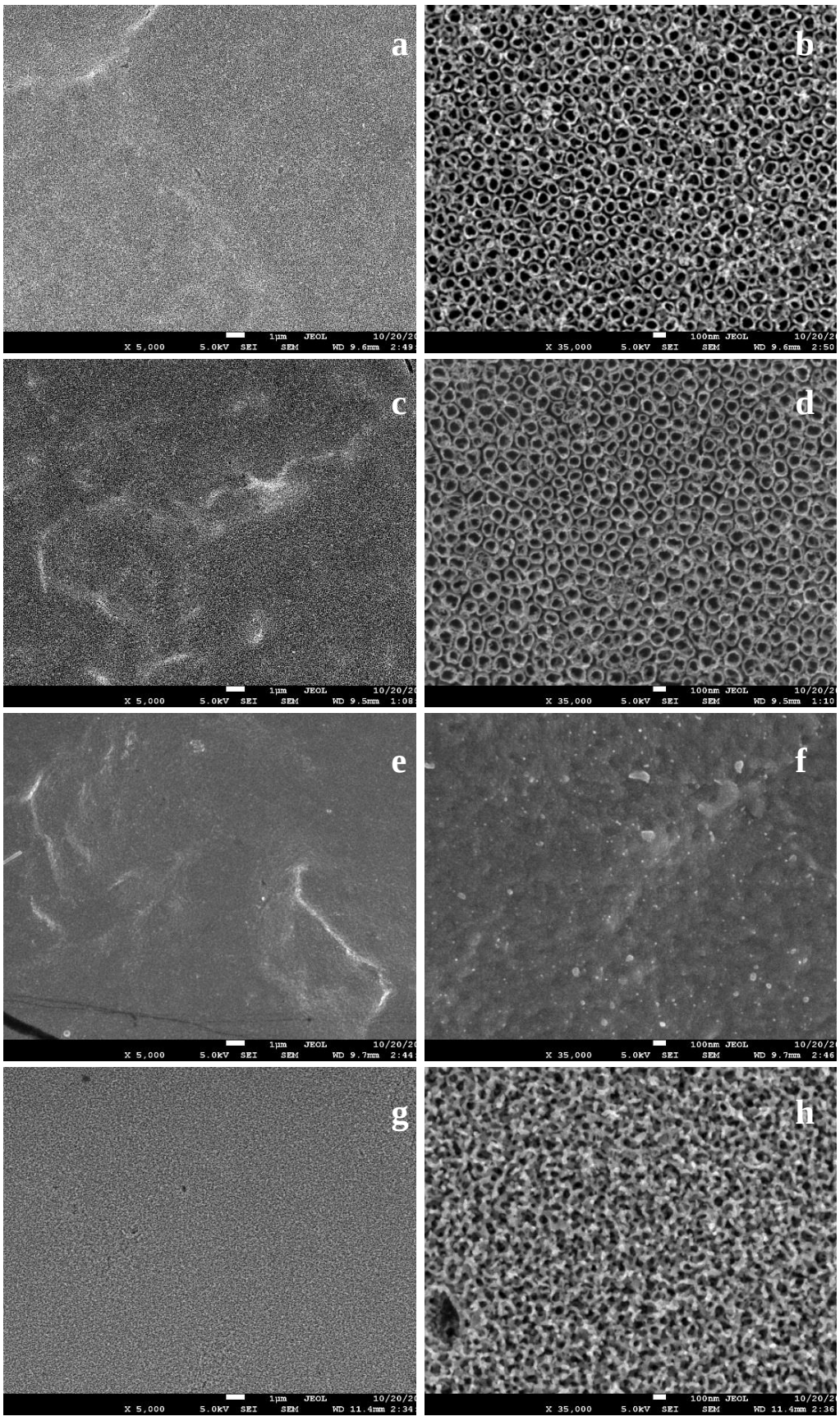

Figure 4.8: SEM images of samples produced in electrolyte EHOx including 0.5wt% HF at; a, b) 15 min, c, d) 30 min, e, f) 60 min, g, h) 120 min with 20V.

It was obtained that sample anodized in electrolyte EH at 120 min has more homogenous TNTAs than the other samples. In contrast to our results, Erol et al reported that uniform titanium dioxide nanoporous structures were formed on the samples anodized in similar electrolyte at parameters 20V, 240 min, 20^{o}C [82]. On the other hand, formation of TNTAs was observed in samples anodized in electrolyte EHOx at 15 and 30 min according to Figure 4.8b, d. Alteration of the tube structure was determined sample anodized in electrolyte EHOx at 60 and 120 min as seen in Figure 4.8f, h. However, Su et al reported that homogenous and smooth TNTAs were produced with similar electrolyte (using NH_4F instead of HF) with 20V at 60 min [55].

As a result of all the morphological evaluations, it can be declared that the uniform and homogenously distributed TNTAs were obtained with the following parameters for electrolyte EH: anodization voltage, time and HF concentrations 20V, 120 min and 0.5wt%, respectively. If the morphologies for the samples anodized in EHOx with various time were considered, it can be stated that intended structure were not obtained with longer anodization times. However, these structures were obtained in only 30 minutes. As mentioned before we have focused on the incorporation of boron in the TNTA structure. With this manner **20 *V,* 120 *min and* 0.5 *wt % HF*** were chosen as the further anodization parameters for both electrolyte EH and EHOx so as to provide sufficient time for doping process and comparison of the results.

4.2.2. Boron doped titanium dioxide nanotube arrays

The SEM images of samples anodized with 20 V at 120 min in electrolyte EHB and EHOxB which were defined in experimental studies were shown in Figure 4.9 and 4.10. According to the figures formation of uniform and homogenously distributed TNTAs was observed for all doped samples. Therefore, it can be stated that the doping agent did not cause any change on tube structure.

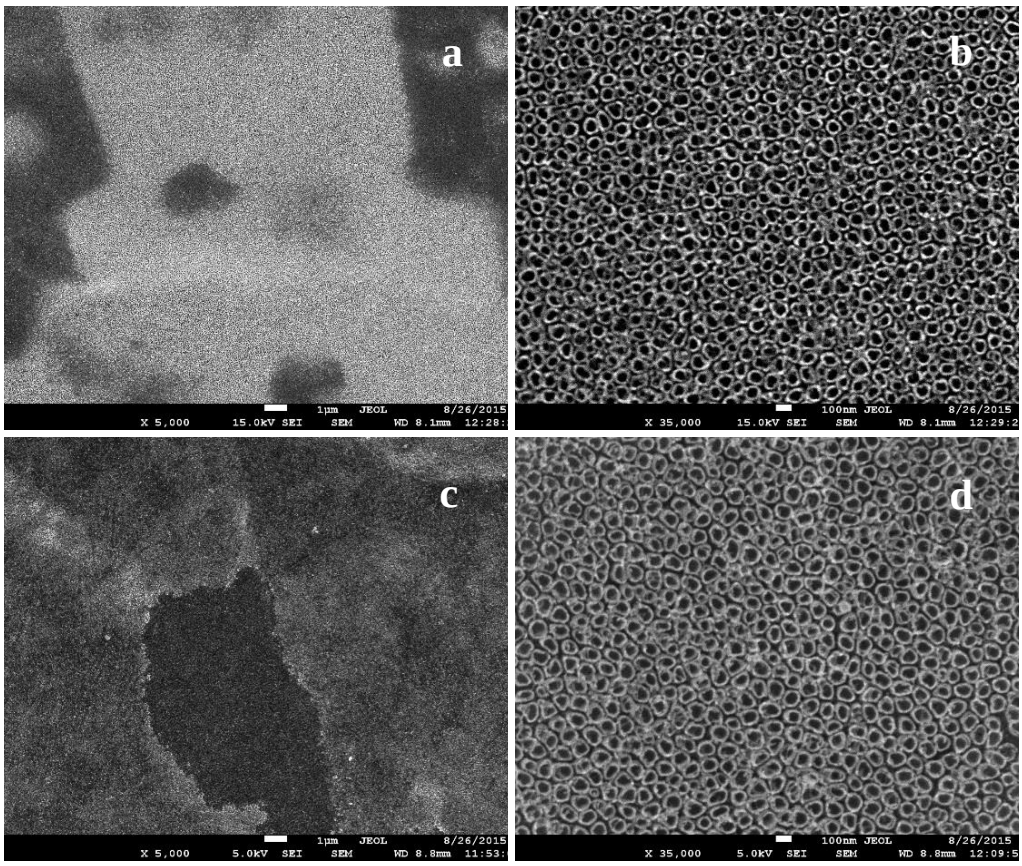

Figure 4.9: SEM images of samples produced in electrolyte EHB with various $NaBF_4$ content (wt%); a, b) 0.015; c, d) 0.030.

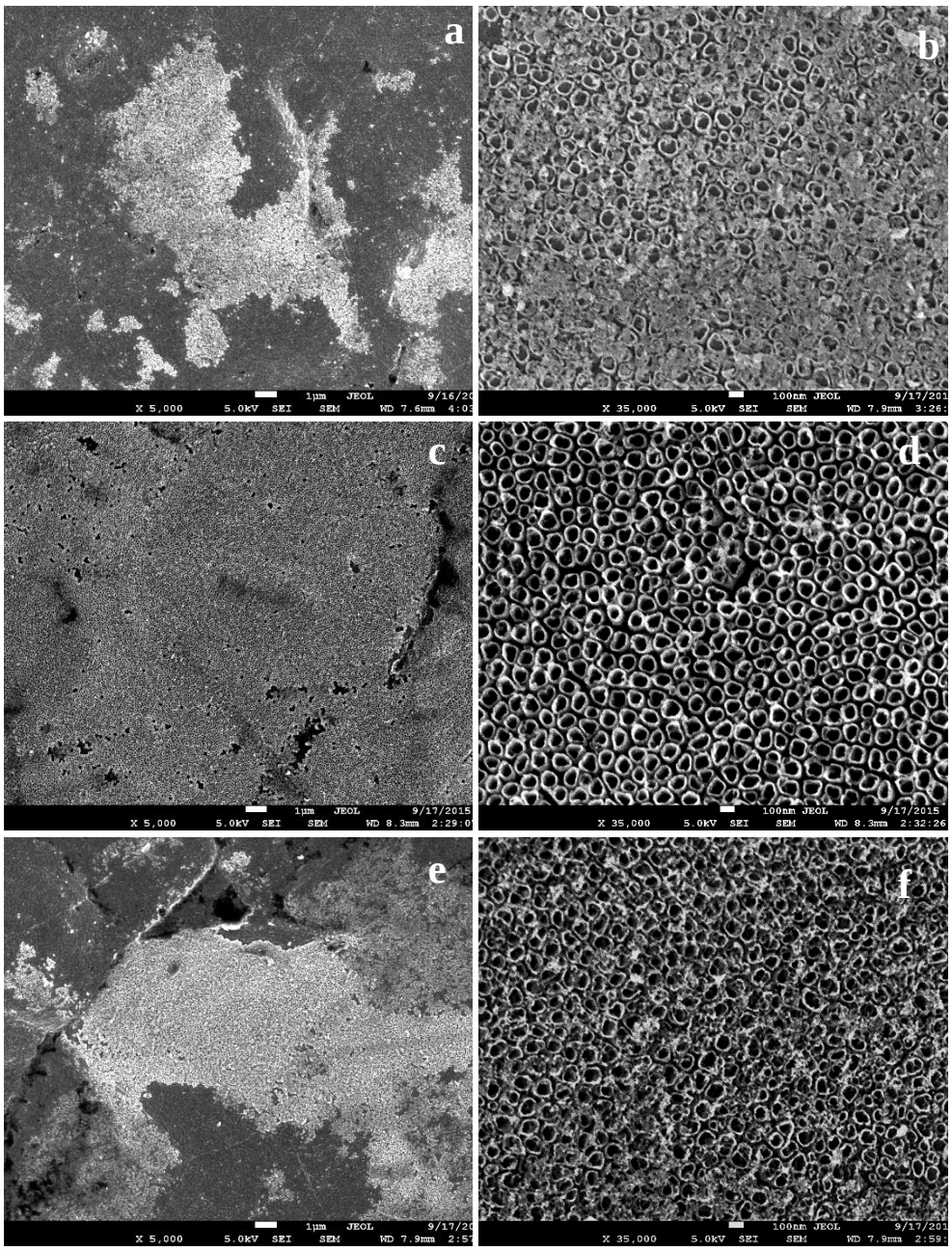

Figure 4. 10: SEM images of samples produced in electrolyte EHOxB with various $NaBF_4$ content (wt%); a, b) 0.2; c, d) 0.5; e, f) 1.0.

In addition to SEM observations, amounts of wt% B doped in TiO_2 lattice were also determined by energy-dispersive X-ray spectroscopy (EDS) with similar approach to references [98, 99], as given in Table 4.1. According to the table it can be expressed that the detected (also cannot be detected in some samples) amounts were not found to be in sequence with the intended ratios given in Table 3.3 and Table 3.4 thanks to light molecular weight and low ratio of boron in the structure and the electrolytes. Although Lu et al reported that they could accomplish to incorporate boron into

TNTAs by using an electrolyte similar to EHB, our results pointed out that this electrolyte is not appropriate for the production of B-TNTAs [59].

In contrast to EHB electrolytes, the EDS results of the samples anodized in electrolyte EHOxB showed that maximum boron content detection is provided with sample B05-Ox-V20T120C50 and these electrolyte and process are more applicable to dope boron into structure with oxalic acid based electrolytes.

Table 4.1: EDS elemental weight % analysis of all samples.

Electrolyte	Element (wt%) → Sample↓	B	O	Ti
EHB	V20T120C50	0	29.73	69.44
	B015-V20T120C50	*ND	24.74	76.26
	B030-V20T120C50	0.05	21.72	78.24
EHOxB	Ox-V20T120C50	0	30.145	69.85
	B02-Ox-V20T120C50	*ND	20.71	79.29
	B05-Ox-v20T120C50	1.35	15.80	81.39
	B10-Ox-V20T120C50	0.18	18.32	81.49

*ND: No detection

In addition to these, weight percentage of incorporated boron into the structure is quite low account although atomic radius of boron is smaller than titanium and oxygen. Boron cannot be incorporated into the structure more than the results because to provide boron atom using dopant agent $NaBF_4$ is found as the form of BF_4^- in electrolyte.

In literature, Su et al performed CVD assisted boron doping into as anodized TNTA through a two steps operation with oxalic acid based electrolyte [55, 58]. In comparison, it can be declared that boron incorporation in to structure was successfully performed by our approach through a one step process (anodization) in a more convenient way (Table 4.2).

Figure 4.13 and 4.14 show AFM profiles, 2-D and 3-D scanning areas ($62.3 \times 62.3 mm^2$) of samples anodized in electrolyte EHB and EHOxB, respectively. According to the images it can be stated that almost every sample had similar surfaces and change in the boron ratio did not affect the morphologies which are in a good agreement with the SEM images.

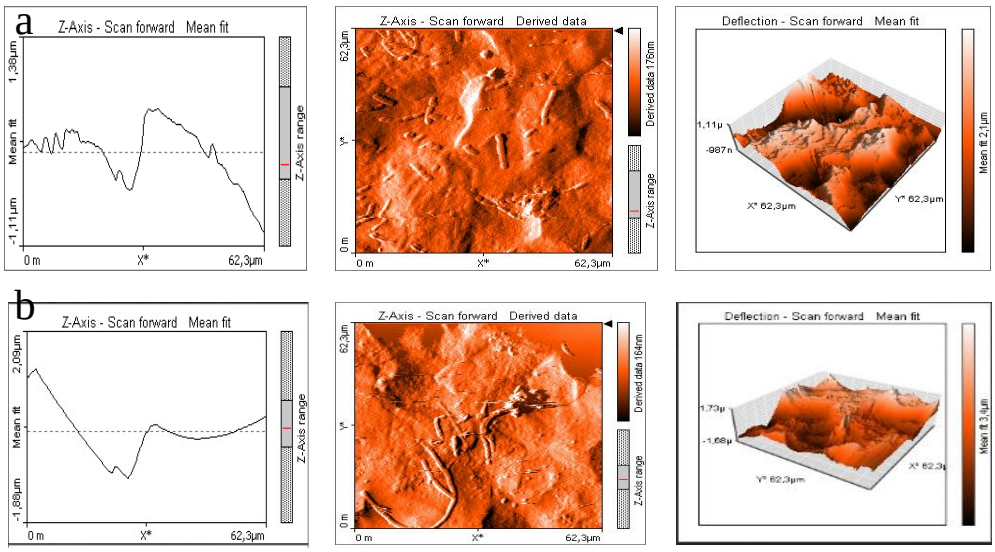

Figure 4.11 : AFM analysis of samples produced in electrolyte EHB with various $NaBF_4$ content (wt%); a) 0.015; b) 0.030.

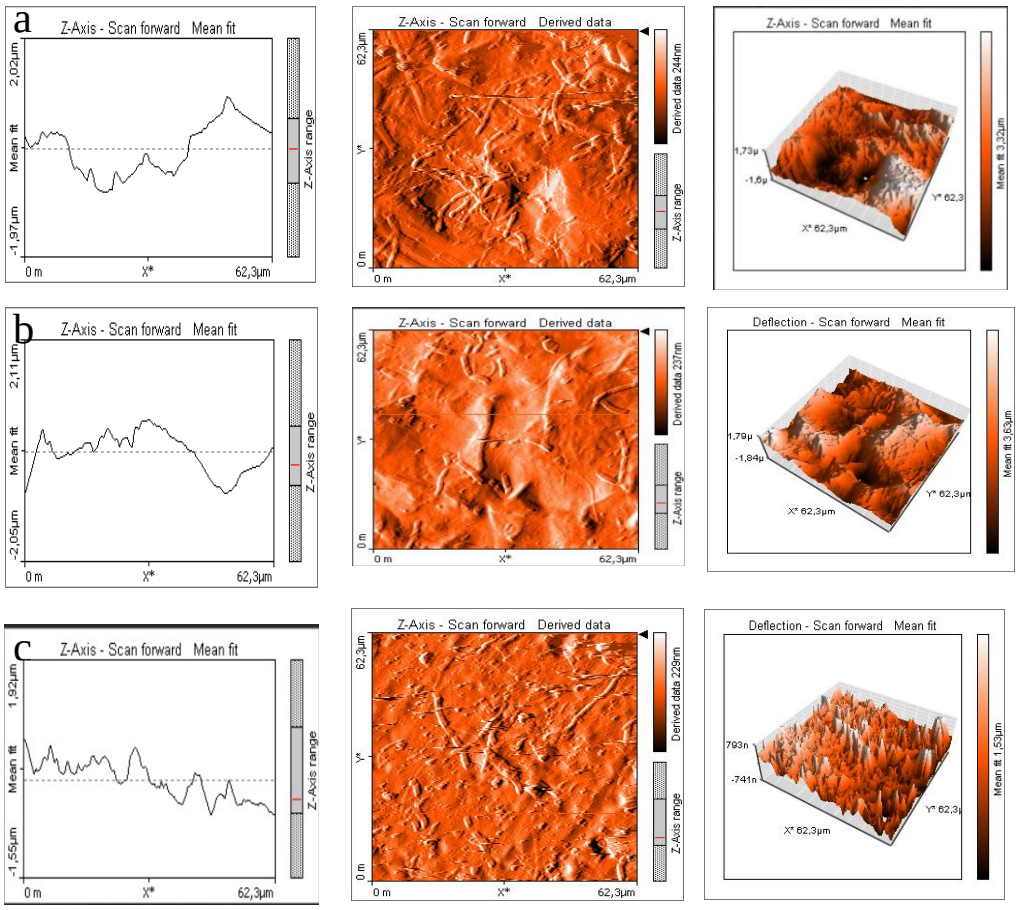

Figure 4.12: AFM analysis of samples produced in electrolyte EHOxB with various $NaBF_4$ content (wt%); a) 0.2; b) 0.5; c) 1.0.

4.3. Optical Analysis

As mentioned elsewhere the main objective of this research is to constitute B-TNTAs with desired optical and enhanced photocatalytical properties. As known boron is an important doping element for tailoring band gap of TiO_2 [55-59].With this motivation, optical characterizations of TNTAs produced with optimum anodizing parameters in electrolytes EH, EHOx, EHB and EHOxB were performed via diffuse reflectance spectra (DRS). The DRS spectra of samples anodized in electrolyte EHB and EHOxB (absorbance v.s wavelength) were given in Figure 4.13 and 4.14, respectively. Therefore, band gap energy values were calculated by using equation mentioned previously in experimental section and were listed in Table 4.2.

Table 4.2: Band gap values of samples anodized in EHB and EHOxB.

Electrolyte	**Sample**	**Wavelength of intercept (nm)**	**E_g (eV)**
EHB	V20T120C50	358.37	3.46
	B015-V20T120C50	378.64	3.27
	B030-V20T120C50	372.67	3.32
EHOxB	Ox-V20T120C50	372.00	3.32
	B02-Ox-V20T120C50	370.49	3.34
	B05-Ox-v20T120C50	409.19	3.03
	B10-Ox-V20T120C50	389.71	3.30

The band-gap energy of anatase TiO_2 is 3.2 eV, as reported by Maruska and Ghosh [103]. However, in the present study, the band-gap energies of TNTAs without doping are 3.46 eV and 3.32 eV for samples anodized in EH and EHOx, respectively which are slightly higher than Maruska and Ghosh's value of 3.2 eV, but lower than reported value 3.6 eV by Tiginyanu [37]. Ren et al reported that band gap energy of p-type NiO (nickel oxide) loaded porous titanium dioxide sheets prepared via freeze tape-casting was evaluated to be 3.02 eV [99]. Reddy et al reported that band gap energies all of these; bulk polycrystalline titanium dioxide in the form of a commercial powder, as-prepared titanium dioxide by using titanium tetrachloride and hydrazine hydrate and hydrogen annealed polycrystalline titanium dioxide were estimated 3.2 eV, 3.36 eV and 3.32 eV, respectively [100]. In addition to these studies, Lu et al reported that bandgap energy of TNTAs produced by anodization

could be reduced from 3.33 eV to 3.10 eV (refer to pure titanium and doped TiO_2, respectively) by doping boron [59]. The differences in the literature are thought to be because of the materials' form (film, powder, fiber and etc), measurement conditions, instrumentation, formulation and etc. In spite of the inconsistency with literature, the projected decrease for B doping significantly observed in the present study. The decrease can be ascribed to the energy states that arise in the forbidden zone of energy resulted from the presence of transition metals and oxygen vacancies in TiO_2 lattice.

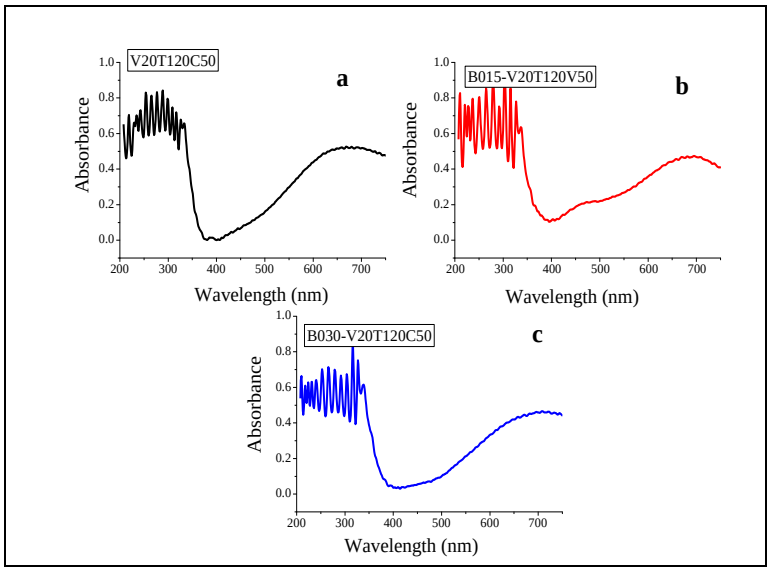

Figure 4.13: UV-Visible diffuse reflectance spectra of samples produced in electrolyte EHB with various $NaBF_4$ content (wt%); a) 0.0; b) 0.015; c) 0.030.

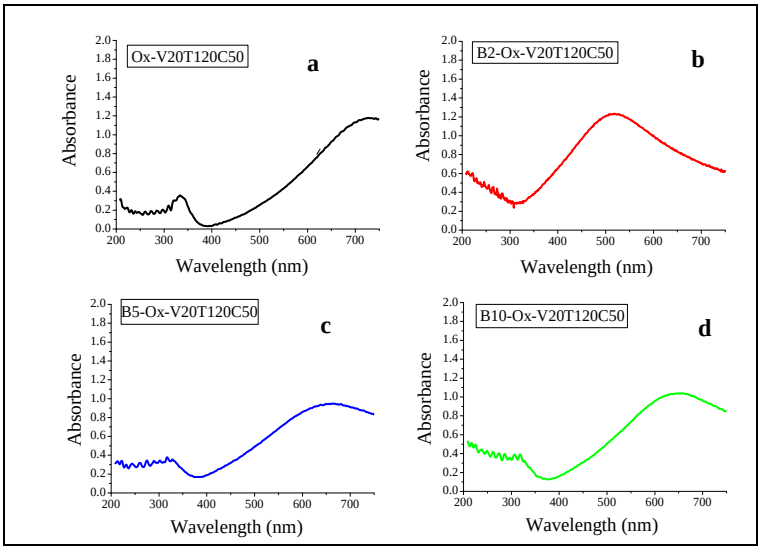

Figure 4.14: UV-Visible diffuse reflectance spectra of produced in electrolyte EHOxB with various $NaBF_4$ content (wt%); a)0.0; b)0.2; c) 0.5; d) 1.0.

4.4. Photocatalytical Analysis

Initially photocatalytic degradation of aqueous MB solutions catalyzed with samples anodized in electrolyte EHB and EHOxB on MB using the previously mentioned system (Figure 3.8). The changes in colour (decreasing concentration) thanks to the degradation reactions were monitored for different intervals by using UV-Vis spectrophotometer to obtain absorbance spectrum. It is important to note that measured maximum absorbance values at 664 nm wavelength between 0–360 minutes of irradiation were converted to molarities using the Lambert-Beer relation given in experimental section.

As mentioned before, rate of a photochemical reaction is important for any industrial reactor design and applications. Photocatalytical oxidation kinetics of many organic compounds such as MB, referred to Langmuir–Hinshelwood kinetics model (L–H) since the compound was adsorbed on the catalyst surface and the reaction is surface controlled. With this manner; some important units C, C_0, m and t must be defined as the instant molarity, starting molarity, rate constant and time respectively [101]. The results depicted in Figure 4.15 a, b indicate that the kinetics of photocatalytic reaction fit the Langmuir–Hinshelwood kinetics model for samples anodized in electrolyte EHB and EHOxB, respectively. Regarding to the kinetic data plotted in Figure 4.15a,b, it can be inferred that the best photocatalytical performance was obtained with sample B05-Ox-V20T120C50 with linear fitted functions according to the Langmuir–Hinshelwood. According to the linear fitting process, the rate constants and R^2 were calculated as in Table 4.3.

Table 4.3: Kinetic data of samples anodized in electrolyte EHB and EHOxB.

Electrolyte	Sample	Kinetic Constant, k (h^{-1})	R^2
EHB	V20T120C50	0.15	0.901
	B015-V20T120C50	0.114	0.8577
	B030-V20T120C50	0.072	0.6259
EHOxB	Ox-V20T120C50	0.108	0.9878
	B02-Ox-V20T120C50	0.078	0.5927
	B05-Ox-V20T120C50	0.126	0.9496
	B10-Ox-V20T120C50	0.09	0.8763

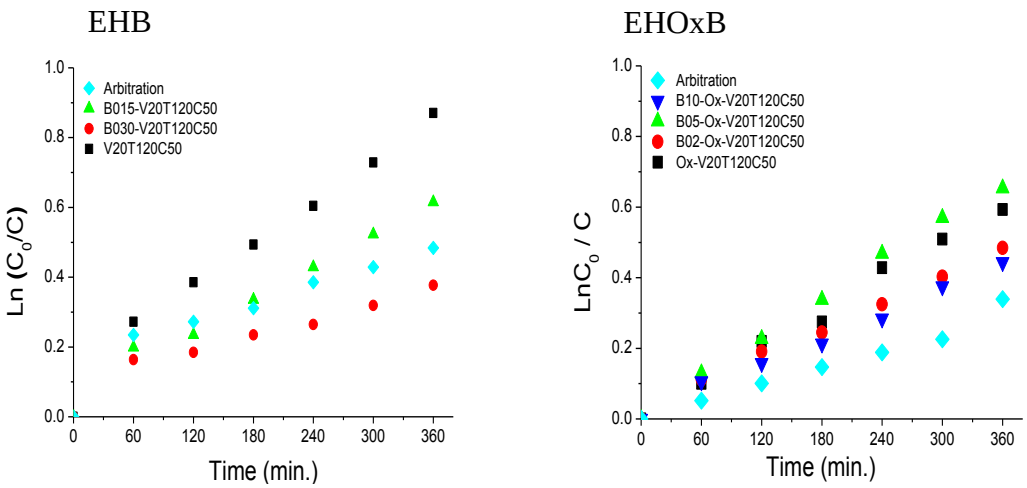

Figure 4.15: Reaction kinetics' comparison of samples anodized in electrolytes EHB and EHOxB.

In the light of these result, it can be stated that the best photocatalytic kinetic was observed with B05-Ox-V20T120C50. This kinetic datum show to us that the kinetics of the samples anodized in EHB exhibited lower values than the samples anodized in EHOxB. HF based electrolytes cause to obtain short nanotubes [81] since it could affect current density, in contrast to this, $C_2H_2O_4.H_2O$ could provide nanotubes breakdown arising from high current density [57] Therefore, it can be expressed that photocatalytic efficiency depend on length of nanotubes. If the kinetics of the samples anodized in EHB are compared with each other, it can be expressed that the kinetic of V20T120C50 sample is better than B030-V20T120C50 since this example does not have a homogenous nanotube distribution (Figure 4.9 c). If the kinetics of the samples anodized in EHOxB are compared with each other, it can be seen that predicted results were obtained with these samples so kinetic of B5-Ox-V20T120C50 sample was found to be better than Ox-V20T120C50. Furthermore, our results cannot be compared with any studies in literature because there are a lot of parameters effected photocatalytic properties as surface morphology, crystalline structure, band configuration, grain size, sample size, light intensity, and etc which are not exactly same or comparable with ours.

5. CONCLUSION

In this study, fabrication of boron doped titanium dioxide nanotube arrays was successfully performed through a one step electrochemical anodization process in two different electrolytes including dopant agents. Experimental work was carried out in two stages to produce TNTAs and B-TNTAs respectively.

In first stage, optimum anodization parameters (V, t, C) to obtain uniform nanotube structure on titanium substrates surfaces were determined in both electrolytes EH (HF/H_2O) and EHOx ($C_2H_2O_4 \cdot 2H_2O/HF/H_2O$). Titanium substrates were prepared with 10 mm thickness and 15 mm diameter. The substrates were cleaned with solution including acetone, ethanol and pure water in ultrasonic bath. Cleaned substrates were made etching with solution including hydrogen floride, nitric acid and pure water for 10-12 second. After that, the substrates were rinsed with pure water. Then, they were anodized with different parameters. Firstly, anodization was performed for different voltages; 10, 20, 30 and 40V in electrolytes including 0.5 wt% HF at 30 min. Samples were annealed at 450^0C for 2 h. Secondly, it was performed at different times; 15, 60 and 120 minutes for 20V in electrolytes including 0.5 wt% HF and samples were annealed at 450^0C for 2 h. Finally, it was performed in electrolytes including different concentration of HF for 20V at 30min and samples were annealed at 450^0C for 2 h. All samples and parameters were evaluated according to SEM observations. Uniform and homogenous nanotube structure was obtained with **20V, 120 minutes, 0.5wt % HF** anodization parameters for electrolyte **EH.** On the other hand, uniform nanotubes were obtained with **20V, 30 minutes, 0.5 wt% HF** anodization parameters for electrolyte **EHOx.** The determined optimum duration (30 minutes) was thought to be not enough for doping process. Thus, final optimum parameters for second stage were chosen as **20V, 120 minutes, 0.5wt % HF** for incorporation.

In second stage, B-TNTAs were fabricated with optimum anodization parameters in both electrolytes EHB ($HF/H_2O/NaBF_4$) and EHOxB ($C_2H_2O_4 \cdot 2H_2O/HF/H_2O/NaBF_4$) on the substrates prepared and cleaned with same procedure in first stage. Then, the substrates were anodized in five different electrolytes (EHB including 0.015, 0.030 wt% $NaBF_4$ and EHOxB including 0.2, 0.5, 1.0 wt% $NaBF_4$) with previously determined optimum parameters. Anodized samples

were heated up to 450ºC for phase transformation from amorphous to anatase structure. The samples were characterized by XRD, AFM, SEM, EDS, DRS to express the effect of boron doping into TNTAs.

XRD results points to the fact that boron doping in to structure did not effect on transformation of anatase phase. Each XRD pattern had weak **anatase** and dominant **titanium** peaks regarding to the thicknesses of anodized layers. AFM images show that almost every sample had similar surfaces and change in the boron ratio did not affect the morphologies. Formation of **nanotube structures** were observed with SEM images of almost every sample. EDS results represents that the best incorporation of boron into the structure **(1.35 wt %)** was performed in electrolyte **EHOxB** including **0.5 wt% $NaBF_4$**. It can be supported with DRS results. According to the results, decreasing band gap energy value **(as from 3.32 to 3.03 eV)** was obtained with the sample anodized in this electrolyte EHOxB including 0.5 wt% $NaBF_4$. Photocatalytic activity of TNTAs and B-TNTAs were tested under UV light. According to the results, the best activity was recorded sample anodized in electrolyte EHOxB including 0.5 wt% $NaBF_4$ due to it has kinetic constant as **0.126 h^{-1}**.

In this study, the results lead us to the conclusion that boron incorporation into the structure of sample anodized was efficiently performed in the electrolyte including 0.5wt % $NaBF_4$ without homogeneous nanotube distributions. Oxalic acid presence in electrolyte can be investigated to produce more uniform and homogenously distributed nanotube structures since it could prevent nanotubes breakdown caused by high current density and it could provide boron incorporation into the structure efficiently. Different amount of dopant between 0.5-1.0 weight percent $NaBF_4$ can be studied in electrolyte EHOxB for further studies. So finally it can be inferred that the investigated samples as catalyst can be used for photocatalytic reactors by developing with new studies.

6. REFERENCES

[1] C. Fernandez, M.S. Larrechi, M.P. Callao, Trends Anal. Chem. 29 (2010) 1202–1211.

[2] H. Shu, J. Xie, H. Xu, H. Li, Z. Gu, G. Sun, Y. Xu, J. Alloys Compd. 496 (2010) 633–637.

[3] A. Fujishima, T.N. Rao, D.A. Tryk, ‘’Titanium dioxide photocatalysis’’, J. Photochem. Photobiol. C 1 (2000) 1–21.

[4] A. Fujishima, X. Zhang, D.A. Tryk, ‘’TiO2 photocatalysis and related surface phenomena’’, Surf. Sci. Rep. 63 (2008) 515–582.

[5] K. Hashimoto, H. Irie, A. Fujishima, ‘’TiO2 photocatalysis: a historical overview and future prospects’’, Jpn. J. Appl. Phys. 44 (2005) 8269–8285

[6] A. Fujishima, K. Honda, ‘’Electrochemical photolysis of water at a semiconductor electrode’’, Nature 238 (1972) 37–38.

[7] A. Ryu, ‘’Recent progress on photocatalytic and photoelectrochemical water splitting under visible light irradiation’’, J. Photochem. Photobiol. C 11 (2010)179–209

[8] T. Inoue, A. Fujishima, S. Konishi, K. Honda, ‘’Photoelectrocatalytic reduction of carbon dioxide in aqueous suspensions of semiconductor powders’’, Nature277 (1979) 637–638

[9] L. Caballero, K.A. Whitehead, N.S. Allen, J. Verran, ‘’Inactivation of Escherichia coli on immobilized TiO2 using fluorescent ligh’’, J. Photochem.Photobiol. A 202 (2009) 92–98.

[10] R. Cai, K. Hashimoto, K. Itoh, Y. Kubota, A. Fujishima, Photokilling of malignant cells with ultrafine TiO2 powder, Bull. Chem. Soc. Japan 4 (1991) 1268–1273.

[11] T. Matsunaga, R. Tomoda, T. Nakajima, H. Wake, Photoelectrochemical sterilizationof microbial cells by semiconductor powders, FEMS Microbiol. Lett.29 (1985) 211–214.

[12] C. McCullagh, J. Robertson, D. Bahnemann, P. Robertson, The application of TiO2 photocatalysis for disinfection of water contaminated with pathogenic micro-organisms: a review, Res. Chem. Intermed. 33 (2007)359–375.

[13] J.R. Peller, R.L. Whitman, S. Griffith, P. Harris, C. Peller, J. Scalzitti, TiO2 as a photocatalyst for control of the aquatic invasive alga, Cladophora, undernatural and artificial light, J. Photochem. Photobiol. A 186 (2007) 212–217.

[14] K. Sunada, T. Watanabe, K. Hashimoto, Studies on photokilling of bacteria on TiO2 thin film, J. Photochem. Photobiol. A 156 (2003) 227–233.

[15] A. Fujishima, X. Zhang, Titanium dioxide photocatalysis: present situation andfuture approaches, C. R. Chim. 9 (2006) 750–760.

[16] A. Fujishima, X. Zhang, D.A. Tryk, Heterogeneous photocatalysis: from water photolysis to applications in environmental clean up, Int. J. Hydrogen Energ.32 (2007) 2664–2672.
[17] K. Nakata, B. Liu, Y. Goto, T. Ochiai, M. Sakai, H. Sakai, T. Murakami, M. Abe, A. Fujishima, Visible light responsive electrospun TiO2 fibers embedded with WO3 nanoparticles, Chem. Lett. 40 (2011) 1161–1162.
[18] K. Nakata, B. Liu, Y. Ishikawa, M. Sakai, H. Saito, T. Ochiai, H. Sakai, T. Murakami, M. Abe, K. Takagi, A. Fujishima, Fabrication and photocatalytic propertiesof TiO2 nanotubes
[19] Hoyer P (1996) Formation of a titanium dioxide nanotube array. Langmuir 12:1411–1413
[20] Lingjuan Liu, JunLv, Guangqing Xu, Yan Wang, Kui Xie, Zhong Chen, Yucheng Wu, Uniformly dispersed CdS nanoparticles sensitized TiO_2 nanotube arrays with enhanced visible-light photocatalytic activity and stability, Journal of Solid StateChemistry 208 (2013) 27–34
[21] Imai H, Takei Y, Shimizu K, Matsuda M, Hirashima H (1999) Direct preparation of anatase TiO2 nanotubes in porous alumina membranes. J Mater Chem 9:2971–2972
[22] Michailowski A, Al Mawlwai D, Cheng GS, Moskovits M (2001) Highly regular anatase nanotubule arrays fabricated in porous anodic templates. Chem Phys Lett 349:1–5
[23] Jung JH, Kobayashi H, van Bommel KJC, Shinkai S, Shimizu T (2002) Creation of novel helical ribbon and double-layered nanotube TiO2 structures using an organogel template. Chem Mater 14:1445–1447
[24] Kobayashi S, Hamasaki N, Suzuki M, Kimura M, Shirai H, Hanabusa K (2002) Preparation helical transition-metal oxide tubes using organogelators as structure-directing agents. J Am Chem Soc 124:6550–6551
[25] Tian ZRR, Voigt JA, Liu J, McKenzie B, Xu HF (2003) Large oriented arrays and continuous films of TiO2-based nanotubes. J Am Chem Soc 125:12384–12385
[26] Kasuga T, Hiramatsu M, Hoson A, Sekino T, Niihara K (1998) Formation of titanium oxide nanotube. Langmuir 14:3160–3163
[27] Chen Q, Zhou WZ, Du GH, Peng LH (2002) Trititanate nanotubes made via a single alkali treatment. Adv Mater 14:1208–1211
[28] Yao BD, Chan YF, Zhang XY, Zhang WF, Yang ZY, Wang N (2003) Formation mechanism of TiO2 nanotubes. Appl Phys Lett 82:281–283
[29] Gong D, Grimes CA, Varghese OK, Hu W, Singh RS, Chen Z, Dickey EC (2001) Titanium oxide nanotube arrays prepared by anodic oxidation. J Mater Res 16:3331–3334
[30] Mor GK, Varghese OK, Paulose M, Mukherjee N, Grimes CA (2003) Fabrication of tapered, conical-shaped titania nanotubes. J Mater Res 18:2588–2593
[31] Cai Q, Paulose M, Varghese OK, Grimes CA (2005), The effect of electrolyte composition on the fabrication of self-organized titanium oxide nanotube arrays by anodic oxidation. J Mater Res 20:230–236
[32] Ruan C, Paulose M, Varghese OK, Grimes CA (2006) Enhanced photoelectrochemicalresponsein highly ordered TiO2 nanotube-arrays anodized in boric acid containing electrolyte.Sol Energy Mater Sol Cells 90:1283–1295

[33] Macak JM, Tsuchiya H, Schmuki P (2005) High-aspect-ratio TiO2 nanotubes by anodizationof titanium. Angew Chem Int Ed 44:2100–2102
[34] Macak JM, Tsuchiya H, Taveira L, Aldabergerova S, Schmuki P (2005) Smooth anodic TiO2nanotubes. Angew Chem Int Ed 44:7463–7465
[35] Balaur E, Macak JM, Tsuchiya H, Schmuki P (2005) Wetting behaviour of layers of TiO2 nanotubes with different diameters. J Mater Chem 15:4488–4491
[36] Macak JM, Schmuki P (2006) Anodic growth of self-organized anodic TiO2 nanotubes in viscous electrolytes. Electrochim Acta 52:1258–1264
[37] Ion Tiginyanu, Pavel Topala, Veaceslav Ursaki, Nanostructures and Thin Films for Multifunctional Applications, 2016, Technology & Engineering, page 183.
[38] M. Zhang, J. Wu, DanDan Lu, and J. Yang; Enhanced Visible Light Photocatalytic Activity for TiO2 Nanotube Array Films by Codoping with Tungsten and Nitrogen, Hindawi Publishing Corporation International Journal of PhotoenergyVolume 2013, Article ID 7167, 8 pages.
[39] J.M. Macak, A. Ghicov, Photoelectrochemical properties of N-doped self-organized titania nanotube layers with different thicknesses. J. Mater. Res., Vol. 21, No. 11, Nov 2006
[40] Asma M. Milad, Mohammad B. Kassim, Wan R. Daud, Fabrication of Carbon Doped TiO2 Nanotubes via In-situ Anodization of Ti-foil in AcidicMedium. World Academy of Science, Engineering and Technology Vol:5 2011-02-22
[41] Yanyan Zhang, Wuyou Fu, Haibin Yang, Synthesis and characterization of P-doped TiO2 nanotubes. Thin Solid Films 518 (2009) 99–103
[42] Deliang Li, LinglingLi,Wei Guo, Zhixian Chang, Minghua Lu , Synthesis and characterization of Mo–Sb–S tridopedTiO2 nanoparticles with enhanced visible light photocatalytic activity. Materials Science in Semiconductor Processing 31(2015)530–535
[43] Jun Lv, Lili Su, Honge Wang, Lingjuan Liu, Guangqing Xu, Dongmei Wang, Zhixiang Zheng, YuchengWu, Enhanced visible light photocatalytic activity of TiO2 nanotube arrays modified with CdSe nanoparticles by electro deposition method, Surface &Coatings Technology 242 (2014) 20–28
[44] Jing Li, Chang-Jian Lin, Jun-Tao Li, Ze-Quan Lin, A photoelectrochemical study of CdS modified TiO_2 nanotube arrays as photo anodes for cathodic protection of stainless steel, Thin Solid Films 519 (2011) 5494–5502
[45] Lakshmi BB, Dorhout PK, Martin CR (1997) Sol-gel template synthesis of semiconductor nano structures. Chem Mater 9:857–862
[46] Yibing Xie, Degang Fu, Supercapacitance of ruthenium oxide deposited on titania and titanium substrates, Materials Chemistry and Physics 122 (2010) 23–29
[47] Biplab Sarma, York R. Smith, Swomitra K. Mohanty, Mano Misra, Electrochemical deposition of CdO on anodized TiO2 nanotube arrays for enhanced photoelectrochemical properties, Materials Letters 85 (2012) 33–36
[48] Zhengbo Jiao, Tao Chen, Jinyan Xiong, Teng Wang, Gongxuan Lu, Jinhua Ye & Yingpu Bi, Visible-light-driven photoelectrochemical and photocatalytic performances of Cr-doped SrTiO3/TiO2 hetero structured nanotube arrays, Scientific Reports | 3:2720 | DOI: 10.1038/srep02720
[49] Min Zhang, Juan Wu, Jian Hou, and JianjunYang, Molybdenum and Nitrogen Co-Doped Titanium Dioxide Nanotube Arrays with Enhanced Visible Light

photocatalytic Activity, Science of Advanced Materials, Volume 5, Number 6, June2013 , pp. 535-541(7)

[50] Jiasong Zhong, Jinrong Xu, Qingyao Wang, Nitrogen and vanadiumCo-doped TiO_2 mesosponge layers forenhancement in visible photocatalytic activity, Applied Surface Science 315 (2014) 131–137

[51] X.F. Leia, X.X. Xue, H. Yang, ‘’Preparation and characterization of Ag-doped TiO_2 nanomaterials and their photocatalytic reduction of Cr(VI) under visible light, Applied Surface Science 321 (2014) 396–403

[52] Xiangxin Yang, Chundi Cao, Keith Hohn, Larry Erickson, Ronaldo Maghirang, Dambar Hamal, Kenneth Klabunde, Highly visible-light active C- and V-doped TiO_2 for degradation of acetaldehyde, Journal of Catalysis 252 (2007) 296–302

[53] Haibin Li, Xuechen Duan, GuocongLiu, Lili Li, Synthesis and characterization of copperions surface-doped titanium dioxide nanotubes, Materials Research Bulletin 43 (2008) 1971–1981

[54] Yunchang Liu, Mingyang Xing, Jinlong Zhang, Ti^{3+} and carbon co-doped TiO_2 with improved visible light photocatalytic activity, Chinese Journal of Catalysis 35 (2014) 1511–1519

[55] Yaling Su, Song Han, Xingwang Zhang, Preparation and visible-light-driven photoelectrocatalytic properties of boron-doped TiO_2 nanotubes. Materials Chemistry and Physics 110 (2008) 239–246

[56] W. Zhao,W. Ma, C. Chen, J. Zhao, Z. Shuai, Efficient degradation of toxic organicpollutants with Ni2O3/TiO2−*x*B*x* under visible irradiation, J. Am. Chem. Soc. 126(2004) 4782–4783.

[57] D. Chen, D. Yang, Q. Wang, Z. Jiang, Effects of boron doping on photocatalyticactivity and microstructure of titanium dioxide nanoparticles, Ind. Eng. Chem.Res. 45 (2006) 4110–4116.

[58] Yaling Su, Xingwang Zhang,F–B-codoping of anodized TiO_2 nanotubes using chemical vapor deposition. Electrochemistry Communications 9 (2007) 2291–2298

[59] Na Lu, Huimin Zhao, Characterization of boron-doped TiO_2 nanotube arrays prepared by electrochemical method and its visible light activity. Separation and Purification Technology 62 (2008) 668–673

[60] William D. Callister, Jr., Materials Science and Engineering An Introduction, seventh edition page 679-694.

[61] P.S. Shewale, S.I. Patil, M.D. Uplane, Preparation of fluorine-doped tin oxide films at low substrate temperature by an advanced spray pyrolysis technique, and their characterization, Semicond. Sci. Technol. 25 (2010) 115008.

[62] K. Lv, M. Zhang, C. Liu, G. Liu, H. Li, S. Wen, Y. Chen, S. Ruan, TiO2 ultraviolet detector based on LaAlO3 substrate with low dark current, J. Alloys Comp. 580(2013) 614–617.

[63] J. Phillips, W. Bowen, E. Cagin, W. Wang, 6.03 – Electronic and optoelectronic devices based on semiconducting zinc oxide, comprehensive, Semicond. Sci.Technol. 4 (2011) 101–127.

[64] Mor, G. K.; Varghese, O. K.; Paulose, M.; Shankar, K.; Grimes,C. A. A review on highly ordered, vertically oriented TiO_2 nanotube arrays: fabrication, material properties, and solar energy applications. Sol. EnergyMater. Sol. Cells 2006, *90*, 2011.

[65] Frank, A. J.; Kopidakis, N.; Lagemaat, van, de. Electrons in nanostructured TiO2 solar cells: transport, recombination and photovoltaic properties. J. Coord. Chem. ReV. 2004, *248*, 1165.
[66] Mor, G. K.; Shankar, K.; Paulose, M.; Varghese, O. K.; Grimes,C. A. Use of highly-ordered TiO2 nanotube arrays in dye-sensitized solarcells. Nano Lett. 2006, 6, 215.
[67] Varghese, O. K.; Paulose, M.; Shankar, K.; Mor, G. K.; Grimes,C. A. Water-photolysis properties of micron-length highly-ordered titania nanotube-arrays. J. Nanosci. Nanotechnol. 2005, 5, 1158.
[68] Dimitris I. Kondarides, Photocatalysis, http://www.eolss.net/Eolss-sampleAllChapter.aspx .
[69] http://energyzee.blogspot.ru/2013/03/cic-wonder-bulb.html.
[70] Poulomi Roy, Steffen Berger, and Patrik Schmuki; TiO2 Nanotubes: Synthesis and Applications. Angew. Chem. Int. Ed. 2011, 50, 2904 – 2939
[71] Mineral Structure and Property Data; TiO_2 Group-University of Colorado
[72] Craig A. Grimes, Gopal K. Mor, TiO_2 Nanotube Arrays Synthesis, Properties and Applications, DOI 10.1007/978-1-4419-0068-5 , Chapter 2, p.68.
[73] T. Mathews, R.P. Antony© Springer International Publishing Switzerland 2015 S. Babu Krishna Moorthy (ed.), Thin Film Structures in Energy Applications,DOI 10.1007/978-3-319-14774-1_5
[74] Daimei Chen, Zhongyi Jiang, Jiaqing Geng, Qun Wang, and Dong Yang; Carbon and Nitrogen Co-doped TiO_2 with Enhanced Visible-Light Photocatalytic Activity, Ind. Eng. Chem. Res. 2007,46, 2741-2746 2741.
[75] Kazuhito Hashimoto, Hiroshi Irie and Akira Fujishima, TiO_2 Photocatalysis: A historical Overview and Future Prospects, Japanese Journal of Applied Physics Vol.44, No.12 (2005) pp.8269-8285.
[76] T.Dikici, S.Yıldırım, M.Yurddaskal, M.Erol, A comparative study on the photocatalytic activities of microporous and nanoporous TiO_2 layers Prepared by electrochemical anodization, Surface & Coatings Technology 263 (2015) 1-7
[77] Jiasong Zhong, Jinrong Xu, Qingyao Wang, Nitrogen and vanadium Co-doped TiO_2 mesosponge layers forenhancement in visible photocatalytic activity, Applied Surface Science 315 (2014) 131–137
[78] Craig A. Grimes, Gopal K. Mor, TiO_2 Nanotube Arrays Synthesis, Properties and Applications, DOI 10.1007/978-1-4419-0068-5 , Chapter 1, p.3.
[79] Craig A. Grimes, Gopal K. Mor, TiO_2 Nanotube Arrays Synthesis, Properties and Applications, DOI 10.1007/978-1-4419-0068-5 , Chapter 1,2,3, p.27-380.
[80] Thomas Cottineau, Nicolas Béalu, Pierre-Alexandre Gross; One step synthesis of niobium doped titanium dioxide nanotubes arrays by anodization to form (N,Nb) co-doped TiO_2 with an enhanced visible light photoelectrochemical activity. Electronic Supplementary Material (ESI) for Journal of Materials Chemistry A This journal is © The Royal Society of Chemistry 2012
[81] T. Dikici, M.Erol, M.Toparli, E.Celik ; Characterization and photocatalytic properties of nanoporous titanium dioxide layer fabricated on pure titanium substrates by the anodic oxidation process, Ceramics International40(2014)1587–1591.
[82] M.Erol, T.Dikici, M.Toparli, Erdal Celik; The effect of anodization parameters on the formation of nanoporous TiO2 layers and their

photocatalytic activities, Journal of Alloys and Compounds 604 (2014) 66–72
[83] education.mrsec.wisc.edu/nanoquest.
[84] gap.http://www.powerguru.org/semiconductor-doping/.
[85] H. Eskandarloo, M. Hashempour, A. Vicenzo, S. Franz, A. Badiei, M. A. Behnajady, M. Bestett ; High-temperature stable anatase-type TiO2nanotube arrays: A study of the structure–activity relationship, Applied Catalysis B: Environmental 185 (2016) 119–132.
[86] S. Demirci, B.Öztürk, S.Yildirim, F.Bakal, M.Erol; Synthesis and comparison of the photocatalytic activities of flame spray pyrolysis and sol–gel derived magnesium oxide nano-scale particles, Materials Sciencein Semiconductor Processing 34 (2015) 154–161.
[87] http://www.ssi.shimadzu.com/products/product.cfm
[88] J. Cenens, R. A. Schoonheydt; Visible spectroscopy of methylene blue on hectorite, laponite B, and barasym in aqueous suspension, Clays and Clay Minerals, Vol. 36, No. 3, 214-224, 1988.
[89] M Yurddaskal, T Dikici, S Yildirim, M Yurddaskal, M Toparli, E Celik, Fabrication and characterization of nanostructured anatase TiO 2 films prepared by electrochemical anodization and their photocatalytic properties, Journal of Alloys and Compounds 651, 59-71.
[90] T.Dikici, S.Yıldırım, M.Yurddaskal, M.Erol; Acomparative study on the photocatalytic activities of microporous and nanoporous TiO2 layers Prepared by electrochemical anodization, Surface & Coatings Technology 263 (2015) 1-7
[91] Q. A. S. Nguyen, Y. V. Bhargava, V. R. Radmilovic , T. M. Devine; Structural study of electrochemically synthesized TiO2 nanotubes via cross-sectional and high-resolution TEM, Electrochimica Acta 54 (2009) 4340–4344.
[92] Matthew R. Sturgeon, PengLai, and Michael Z. Hu, ‘’Acomparative study of anodizedtitania nanotube architecturesin aqueous and nonaqueous solutions’’ http://journals.cambridge.org DOI: 10.1557/jmr.2011.243.
[93] C. Wehrenfennig, C. M. Palumbiny, H. J. Snaith, M. B. Johnston, L. Schmidt-Mende,and L. M. Herz, Fast Charge-Carrier Trapping in TiO2 Nanotubes, Journal of PhysicalChemistry C 2015, 119, 9159−9168. DOI: 10.1021/acs.jpcc.5b01827
[94] QueAnh S. Nguyena, Yash V. Bhargavaa, Velimir R. Radmilovic, Thomas M. Devinea, Structural study of electrochemicallysynthesized TiO2 nanotubes viacross-sectional and high-resolution TEM ElectrochimicaActa 54 (2009) 4340–4344.
[95] A. Valota, D.J. LeClere, P. Skeldon, M. Curioni, T. Hashimoto, S. Berger, J. Kunze, P. Schmuki, G.E. Thompson, Influence of water content on nanotubular anodic titania formed in fluoride/glycerolelectrolytes ElectrochimicaActa 54 (2009) 4321–4327.
[96] Yong-HoonJeong,Won-Gi Kim, Han-CheolChoe, William A. Brantley, Control of nanotube shape and morphology on Ti–Nb(Ta)–Zralloys by varyinganodizing potential, Thin Solid Films 572 (2014) 105–112.
[97] Linda Ingemarsson & Mats Halvarsson, SEM/EDX Analysis of Boron, High Temperature Corrosion Centre-Chalmer University of Technology (2011).
[98] Dr. Jana Berlin, Analysis of Boron with Energy Dispersive X-ray Spectrometre, Advances in Light Element Analysis with SDD Technology, BRUKER

[99] L. Ren, Y. Zeng, D. Jiang, The improved photocatalytic properties of P-type NiO loaded porous TiO2 sheetsprepared via freeze tape-casting, Solid State Sciences 12 (2010) 138–143.
[100] K. Madhusudan Reddy, Sunkara V. Manorama, A. Ramachandra Reddy, Bandgap studies on anatase titanium dioxide nanoparticles, Materials Chemistry and Physics 78 (2002) 239–245.
[101] C.S. Uyguner, M. Bekbolet, Photocatalytic degradation of natural organic matter: Kinetic considerations and light intensity dependence, Int. J.Photoenergy 6 (2004) 73–80.